Polymer 51 (2010) 936–952

Contents lists available at ScienceDirect

Polymer

journal homepage: www.elsevier.com/locate/polymer

Exfoliation of organoclay nanocomposites based on polystyrene-*block*-polyisoprene-*block*-poly(2-vinylpyridine) copolymer: Solution blending versus melt blending

Weibin Zha [a], Chang Dae Han [a,*], Hong Chul Moon [b], Sung Hyun Han [b], Dong Hyun Lee [b], Jin Kon Kim [b,**]

[a] *Department of Polymer Engineering, The University of Akron, Akron, OH 44325, USA*
[b] *National Creative Research Center for Block Copolymer Self-Assembly and Chemical Engineering Department, Pohang University of Science and Technology, P.O. Box 125, Pohang, Kyungbuk 790-784, Republic of Korea*

ARTICLE INFO

Article history:
Received 21 August 2009
Received in revised form
19 December 2009
Accepted 22 December 2009
Available online 4 January 2010

Keywords:
Nanocomposites
Exfoliation
Block copolymer

ABSTRACT

Exfoliated nanocomposites based on polystyrene-*block*-polyisoprene-*block*-poly(2-vinylpyridine) (SI2VP triblock) copolymer were prepared by solution blending and melt blending. Their dispersion characteristics were investigated using transmission electron microscopy, X-ray diffraction, and small-angle X-ray scattering (SAXS). For the study, SI2VP triblock copolymers with varying amounts of poly(2-vinylpyridine) (P2VP) block (3, 5, and 13 wt%) and different molecular weights were synthesized by sequential anionic polymerization. In the preparation of nanocomposites, four different commercial organoclays, treated with a surfactant having quaternary ammonium salt, were employed. It was found from SAXS that the microdomain structure of an SI2VP triblock copolymer having 13 wt% P2VP block (SI2VP-13) transformed from core-shell cylinders into lamellae when it was mixed with an organoclay. It was found further that the solution-blended nanocomposites based on a homogeneous SI2VP triblock copolymer having 5 wt% P2VP block (SI2VP-5) gave rise to an exfoliated morphology, irrespective of the differences in chemical structure of the surfactant residing at the surface of the organoclays, which is attributable to the presence of ion–dipole interactions between the positively charged N^+ ion in the surfactant residing at the surface of the organoclay and the pyridine rings in the P2VP block of SI2VP-5 and SI2VP-13, respectively. Both solution- and melt-blended nanocomposites based on microphase-separated SI2VP-13 having an order–disorder transition temperature (T_{ODT}) of approximately 210 °C also gave rise to exfoliated morphology. However, melt-blended nanocomposite based on a high-molecular-weight SI2VP triblock copolymer having a very high T_{ODT} (estimated to be about 360 °C), which was much higher than the melt blending temperature employed (200 °C), gave rise to very poor dispersion of the aggregates of organoclay. It is concluded that the T_{ODT} of a block copolymer plays a significant role in determining the dispersion characteristics of organoclay nanocomposites prepared by melt blending.

1. Introduction

The ultimate goal for the preparation of nanocomposites is to achieve a very high degree of dispersion (exfoliation) of the aggregates of layered silicates. Here we use the word "exfoliation" in *qualitative* terms, because in almost all situations "perfect (i.e., ideal) exfoliation" of the aggregates of layered silicates is very difficult to achieve, if not impossible. There are three ways of preparing nanocomposites; namely, (1) in situ polymerization of a monomer using an initiator tethered to the silicate surface or copolymerization of monomers using a silicate-anchored bifunctional initiator, (2) solution blending, and (3) melt blending. It is relatively easy to achieve exfoliation of the aggregates of layered silicates in nanocomposites using in situ polymerization, as compared to melt blending. However, more often than not, in situ polymerization for such purposes is not always an option, especially for thermoplastic polymer or elastomer based nanocomposites.

In the past numerous investigators reported on the preparation of nanocomposites. There are too many papers to cite them all here; however, the interested readers are referred to a recent review article [1]. The majority of those studies reported in the literature dealt with the nanocomposites prepared by melt blending layered silicates with such thermoplastic polymers as polystyrene [2–6], polypropylene [7–10], polycarbonate [11–13], poly(ethylene oxide)

* Corresponding author. Tel.: +1 330 972 6468; fax: +1 330 972 5720.
** Corresponding author. Tel.: +82 54 279 2276; fax: +82 54 279 8298.
E-mail addresses: cdhan@uakron.edu (C.D. Han), jkkim@postech.ac.kr (J.K. Kim).

0032-3861/$ – see front matter © 2009 Elsevier Ltd. All rights reserved.
doi:10.1016/j.polymer.2009.12.030

[14–16], and poly(ε-caprolactone) [17,18], because they were readily available commercially. In the preparation of nanocomposites based on commercial thermoplastic polymers, it is fair to state that intercalation of the aggregates of layered silicates has been observed more often than exfoliation.

There are several factors that play important roles in producing exfoliated nanocomposites; namely, (i) the gallery distance of layered silicates, (ii) compatibility between layered silicates and polymer matrix, and (iii) the mobility of macromolecular chains of a polymer matrix to the surface of layered silicates. The mobility (thus viscosity) of the polymer matrix plays a very important role in controlling the effective mixing between a polymer matrix and layered silicates during the preparation of nanocomposites by melt blending. Note that at a given temperature, the viscosity of a polymer is determined by its molecular weight. However, in the literature the important role of melt viscosity (thus the molecular weight) of the polymer matrix in the preparation of nanocomposites by melt blending has hardly been emphasized. This is particularly relevant to the preparation of nanocomposites based on commercial thermoplastic polymers and elastomers.

From the point of view of obtaining markedly enhanced physical/mechanical properties of nanocomposites, exfoliation is preferred to intercalation because exfoliation of the aggregates of layered silicates gives rise to much larger surface areas than intercalation. Note that regardless of the blending methods employed, the requirement for producing exfoliated nanocomposites is to enhance the chemical affinity (or compatibility) between the surface of layered silicates and the polymer matrix, such that strong attractive interactions between the two can take place.

It is well established that layered silicates (e.g., montmorillonite (MMT)) are hydrophilic [19,20]. Therefore, they do not have chemical affinity with hydrophobic organic polymers and thus the two are incompatible. For this reason, much effort has been spent on chemical modification of, for example, MMT, to provide organophilic surfaces of layered silicates which, when mixed with a thermoplastic polymer, enhance compatibility between a chemically modified clay (hereafter referred to as an organoclay) and a polymer matrix. An alternative approach might be to design polymers that might be able to exfoliate the aggregates of MMT or organoclays.

Thus far, a relatively small number of studies have been reported on the preparation of exfoliated nanocomposites based on block copolymers. The preparation of exfoliated nanocomposites based on block copolymers has an advantage over those based on homopolymers or random copolymers, because one of the blocks in a block copolymer can be modified chemically such that the modified block can be made compatible with the surfactant residing at the surface of an organoclay or a block copolymer can be synthesized in such a way that one of the blocks has functionality, providing an opportunity to have strong attractive interactions with the surfactant residing at the surface of an organoclay. In the past, several research groups reported on the preparation of organoclay nanocomposites based on block copolymers. A few research groups [21,22] employed in situ polymerization to prepare exfoliated organoclay nanocomposites based on block copolymers, while others reported on the preparation, via solution blending [23–27], of exfoliated organoclay nanocomposites either based on chemically modified block copolymers [23–25] or based on block copolymers having inherent functionality [26]. Also, several research groups employed solution blending to prepare intercalated nanocomposites based on microphase-separated, nonfunctional block copolymers [28–33].

Very recently, we synthesized a series of polystyrene-*block*-polyisoprene-*block*-poly(2-vinylpyridine) (SI2VP triblock) copolymers with varying amounts of poly(2-vinylpyridine) (P2VP) block and different molecular weights. The SI2VP triblock copolymers were employed in the present study by introducing a polyisoprene block between the PS and P2VP blocks into a rigid S2VP diblock copolymer, which were employed in our previous study [26], to obtain flexible elastomeric triblock copolymers. This chemical modification demonstrates another aspect of flexibility in obtaining exfoliated organoclay nanocomposites based on a flexible thermoplastic SI2VP elastomer. Using each of the SI2VP triblock copolymers we prepared exfoliated nanocomposites by mixing, via solution blending and melt blending, with an organoclay that was treated with quaternary ammonium salt as surfactant giving rise to positively charged N^+ ion. In the preparation of SI2VP-based nanocomposites reported herein, emphasis was placed on investigating the effects of (1) the amount of P2VP block in SI2VP triblock copolymer, (2) the molecular weight of SI2VP triblock copolymer, and (3) melt blending temperature in relation to the order–disorder transition temperature (T_{ODT}) of SI2VP triblock copolymer. To our knowledge, no study has ever been reported on the preparation, via melt blending, of exfoliated organoclay nanocomposites based on microphase-separated block copolymers. In this paper we summarize the highlights of our findings from the investigation.

2. Experimental

2.1. Synthesis and characterization of SI2VP block polymers

We synthesized, via sequential anionic polymerization, three SI2VP triblock copolymers with varying amounts of P2VP block and different molecular weights. The synthesis procedures employed for SI2VP triblock copolymers are essentially the same as the standard synthesis procedures, which are well documented in the literature. Briefly stated, styrene monomer was first polymerized using tetrahydrofuran (THF) as solvent and *sec*-butyllithium as initiator, followed by the polymerization of isoprene monomer sequentially to the living end of polystyrene block, yielding a living SI diblock copolymer. Then, 2-vinylpryidine was polymerized sequentially to the living end of the polyisoprene block, yielding an SI2VP triblock copolymer. The compositions of the SI2VP triblock copolymers synthesized were determined using ^{1}H NMR spectroscopy and the molecular weight was determined against polystyrene standards using gel permeation chromatography. Table 1 gives a summary of the molecular characteristics of the SI2VP triblock copolymers synthesized.

2.2. Preparation of nanocomposites

To prepare nanocomposites we employed natural clay (montmorillonite MMT, Southern Clay Products), and four different organoclays: Cloisite 30B®, Cloisite 10A®, Cloisite 15A®, and Cloisite 25A® (Southern Clay Products). The chemical structures of the surfactants residing at the surface of each organoclay are shown in Table 2 [34]. Also given in Table 2 is the gallery distance (d_{001} spacing) of each organoclay employed. Note in Table 2 that N^+ ion in the chemical structure of each surfactant denotes quaternary ammonium salt, T denotes tallow consisting of 65% C18, 30% C16,

Table 1
Molecular characteristics of block polymers synthesized in this study.

Sample code	M_w	M_n	Composition (wt%)			T_{ODT} (°C)
			w_{PS}	w_{PI}	w_{P2VP}	
SI2VP-5	2.21×10^4	1.93×10^4	47.5	47.5	5	disordered
SI2VP-13	2.47×10^4	2.23×10^4	43.0	44.0	13	210
SI2VP-3H	9.63×10^4	9.25×10^4	48.5	48.5	3	>220

Table 2
Chemical structures of surfactants residing at the surface of organoclay and the mean interlayer spacing (d_{001}) of organoclays employed in this study (Based on the technical bulletin of Southern Clay Products).

Sample code	Chemical structure of surfactant[a]		d_{001} (nm)
Cloisite 30B®	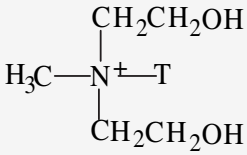	MT2EtOH (90 meq/100 g)	1.85
Cloisite 10A®	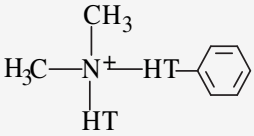	2MBHT (125 meq/100 g)	1.92
Cloisite 15A®	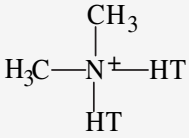	2M2HT (125 meq/100 g)	3.15
Cloisite 25A®	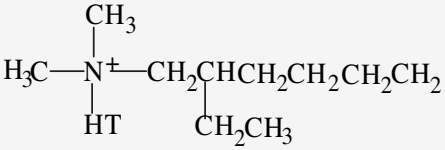	2M2HT8 (125 meq/100 g)	1.86

[a] T in the chemical structure of surfactant denotes tallow consisting of ca. 65% C18, ca. 30% C16, and ca. 5% C14. HT in the chemical structure of surfactant denotes hydrogenatedtallow consisting of ca. 65% C18, ca. 30% C16, and ca. 5% C14. MT2EtOH is methyl tallow bis-2-hydroxyethyl quaternary ammonium ion. 2MBHT is dimethyl benzyl hydrogenated tallow quaternary ammonium ion. 2M2HT is dimethyl dihydrogenated tallow quaternary ammonium ion. 2MHTL8 is dimethyl hydrogenated tallow 2-ethylhexyl quaternary ammonium ion.

and 5% C14, and HT denotes hydrogenated tallow. We were informed by Southern Clay Products that the amount of surfactant residing at the surface of each organoclay is approximately 32 wt% (here wt% denotes the weight percent of the surfactant applied to an organoclay, which was calculated from the amounts of ash collected after burning for 1 h), and 100% of Na^+ ions in MMT have been exchanged. According to the Technical Properties Bulletin [34] from Southern Clay Products, the amount of surfactant MT2EtOH residing at the surface of Cloisite 30B® is 90 meq/100 g and the amount of surfactant 2M2HT residing at the surface of Cloisite 15A® is 125 meq/100 g. We have been informed from Southern Clay Products that an extremely small amount of excess surfactant is present at the surface of Cloisite 30B®, while about 30% excess surfactant is present at the surface of Cloisite 15A®, and that excess amount of surfactant residing at the surface of Cloisite 15A® can be removed when washed with methanol.

In this study we employed both solution blending and melt blending to prepare organoclay nanocomposites based on SI2VP triblock copolymers. Solution blending was employed to prepare organoclay nanocomposites based on SI2VP-5 and SI2VP-13, respectively, and melt blending was employed to prepare organoclay nanocomposites based on SI2VP-13 and SI2VP-3H, respectively. For the preparation of organoclay nanocomposites using solution blending, a predetermined amount of a SI2VP triblock copolymer was dissolved in a co-solvent of THF and water (90:10 v:v), and then an organoclay in a co-solvent of THF/water mixture was added slowly, while stirring vigorously under sonication, into the polymer solution, at room temperature for 15 min. This mixture was evaporated slowly under constant stirring for 48 h. The nanocomposites were dried completely in a vacuum oven at temperatures well above the boiling point of the solvent and also at ca. 20 °C above the glass transition temperature (T_g) of the polymer until no weight changes were detected. Table 3 gives a summary of sample codes of the solution-blended and melt-blended nanocomposites prepared. The amount of MMT or organoclay used was 5 wt% in all nanocomposites prepared, except for (SI2VP-13)/Cloisite 30B®-10 which contains 10 wt% Cloisite 30B®. For the preparation of organoclay nanocomposites using melt blending, we employed a twin-screw mini-compounder (Thermo Haake) and

Table 3
Sample code, the amount of clay and methods of blending employed in the preparation of nanocomposites.

Sample code of nanocomposite	Amount of clay (wt%)	Method of blending
(SI2VP-5)/MMT	5	solution blending
(SI2VP-5)/Cloisite 10A®	5	solution blending
(SI2VP-5)/Cloisite 15A®	5	solution blending
(SI2VP-5)/Cloisite 25A®	5	solution blending
(SI2VP-5)/Cloisite 30B®	5	solution blending
(SI2VP-13)/MMT	5	solution blending
(SI2VP-13)/Cloisite 15A®	5	solution blending
(SI2VP-13)/Cloisite 30B®	5	solution blending; melt blending
(SI2VP-13)/Cloisite 30B®-10	10	solution blending
(SI2VP-3H)/Cloisite 15A®	3	melt blending
(SEBS-*g*-MA)/Cloisite 30B®	5	melt blending

controlled the residence time ranging from 6 to 8 min by recirculating the compound within the extruder at a screw speed of 180 rpm and the extruder barrel temperature was varied depending on the nanocomposites compounded.

2.3. X-ray diffraction (XRD)

Using a Rigaku X-ray generator operated at 40 kV and 40 mA, XRD patterns were obtained to determine the mean interlayer spacing of the (001) plane (d_{001}) for MMT, four organoclays, and the nanocomposites prepared. The X-ray beam was monochromatized to CuK_α with a graphite crystal. The range of 2θ scanning of X-ray intensity employed was 1.5–10°.

2.4. Transmission electron microscopy (TEM)

TEM images of nanocomposite specimens were taken at room temperature. The ultrathin sectioning (50–70 nm) was performed via cryoultra-microtomy at −80 °C for neat block copolymers which was below the glass transition temperature (T_g = −68 °C) of PI block, and at room temperature for nanocomposite specimens, using a diamond knife on the Reichert Ultracut S low-temperature sectioning system. A transmission electron microscope (JEM1200EX II, JEOL) operated at 120 kV was used to record the morphology of the neat block copolymer specimens stained with osmium tetroxide vapor.

2.5. Oscillatory shear rheometry

An Advanced Rheometric Expansion System (ARES, TA Instruments) was used in the oscillatory mode with a parallel plate fixture (8 mm diameter). Dynamic temperature sweep experiments under isochronal conditions were conducted, i.e., the dynamic storage modulus (G') and dynamic loss modulus (G'') were measured at an angular frequency (ω) of 0.1 rad/s during heating. Data acquisition was accomplished with the aid of a microcomputer interfaced with the rheometer. The temperature control was satisfactory to within ±1 °C. All experiments were conducted under a nitrogen atmosphere to preclude oxidative degradation of the samples.

2.6. Small-angle x-ray scattering (SAXS)

Synchrotron SAXS measurement was performed on beamline 4C1 at the Pohang Light Source (Republic of Korea) where a W/B4C double multilayer monochromator delivered monochromatic X-rays with a wavelength (λ) of 0.1608 nm and a resolution $\Delta\lambda/\lambda \approx 0.01$ onto the sample. A two-dimensional CCD camera (Princeton Instruments, SCX-TE/CCD-1242) was used to collect the scattered X-rays. For the SAXS experiments, SI2VP-5 triblock copolymer sample was annealed at 90 °C for 48 h under vacuum and SI2VP-13 triblock copolymer sample was annealed at 180 °C for 48 h under vacuum. The sample thickness was 1 mm.

3. Results and discussion

3.1. Order–disorder transition temperature and microdomain structure of three SI2VP triblock copolymers employed for the preparation of organoclay nanocomposites

Fig. 1a gives the temperature dependence of storage modulus G' for SI2VP-5, SI2VP-13, and SI2VP-3H (see Table 1 for the molecular characteristics of the three block copolymers), which was obtained from the dynamic temperature sweep experiments under isochronal conditions at an angular frequency (ω) of 0.1 rad/s. Following the empirical rheological criterion suggested by Gouinlock and Porter [35], we conclude from Fig. 1 that SI2VP-5 is a disordered (homogeneous) block copolymer, SI2VP-13 is a microphase-separated block copolymer having a T_{ODT} of approximately 210 °C at which values of G' begin to drop precipitously, and SI2VP-3H is also a microphase-separated block copolymer having a T_{ODT} much higher than 220 °C, the highest experimental temperature employed. T_{ODT} represents the temperature at which the microdomains in a block copolymer disappear

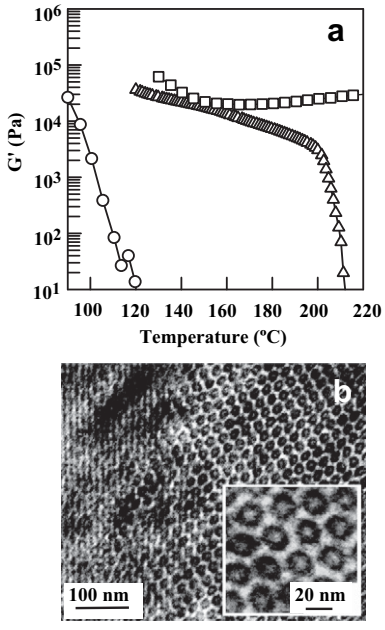

Fig. 1. (a) Variations of dynamic storage modulus G' with temperature during isochronal dynamic temperature sweep experiments at ω = 0.1 rad/s for: (○) SI2VP-5 annealed at 90 °C for 48 h, (△) SI2VP-13 annealed at 180 °C for 48 h, and (□) SI2VP-3H annealed at 120 °C for 48 h. (b) TEM image of SI2VP-13 annealed at 180 °C for 48 h.

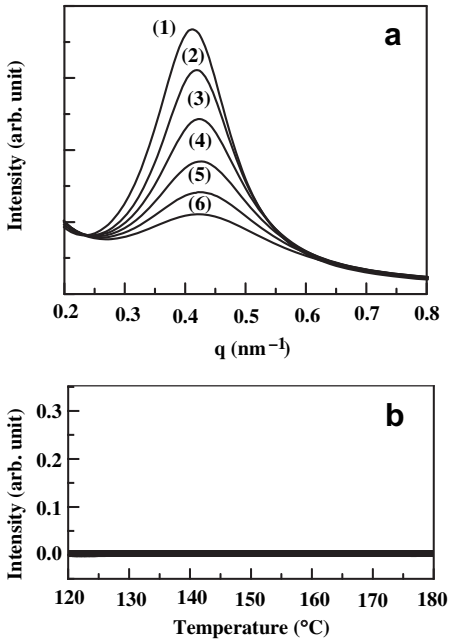

Fig. 2. (a) SAXS profiles of SI2VP-5 at various temperatures (°C): (1) 100, (2) 120, (3) 140, (4) 160, (5) 180, and (6) 200. (b) Temperature dependence of depolarized light scattering intensity of SI2VP-5 during heating at a rate of 0.5 °C/min.

completely. In conducting the dynamic sweep experiments we did not increase measurement temperatures above 220 °C, in order to avoid possible thermal degradation/crosslinking of the polyisoprene (PI) block of SI2VP-3H.

Fig. 1b is a TEM image of SI2VP-13, which was taken after a specimen had been quenched into ice water after having been annealed at 180 °C for 48 h. SI2VP-13 shows hexagonally packed core-shell cylindrical (CSC) microdomains where, due to the selective staining of PI by osmium tetroxide, only the PI block looks dark. We can also clearly see long cylinders on the left side of the image, which are cut along the cylindrical axis direction. Thus, referring to Fig. 1b the PI block becomes the shell, and the core and the matrix consist of P2VP and PS blocks. The shell thickness and the core radius estimated from the inset are about 5 nm and 4 nm, respectively, from which the volume ratio of core and shell is estimated to be about 4.1, which is consistent with the volume ratio 4.2 of PI and P2VP blocks in SI2VP-13 (based on the weight fractions of PI and P2VP blocks given in Table 1 and the specific volumes (cm^3/g) of 1.096 and 0.877 for PI and P2VP, respectively, at 25 °C). Using SAXS and birefringence we reaffirmed that SI2VP-5 is indeed a homogeneous block copolymer over the entire range of temperatures up to 200 °C, as shown in Fig. 2. Namely, the SAXS profiles given in Fig. 2a and the static birefringence given by Fig. 2b indicate that SI2VP-5 is a disordered block copolymer, confirming the conclusion drawn from the temperature dependence of G' observed during the isochronal dynamic temperature sweep experiments (see Fig. 1a). The T_{ODT} of SI2VP-3H is much higher than that of SI2VP-13 because the molecular weight of SI2VP-3H is about three times higher than that of SI2VP-13 (see Table 1). It is well established today that the T_{ODT} of a block copolymer increases with molecular weight [36,37]. The information on the T_{ODT} of SI2VP-13 and SI2VP-3H will be very useful later in this paper to interpret the differences in the dispersion characteristics observed for the two nanocomposites prepared by melt blending, one based on SI2VP-13 and another based on SI2VP-3H.

In addition to the dynamic temperature sweep experiments, we also conducted SAXS and birefringence experiments for SI2VP-13, the results of which are given in Fig. 3. The SAXS profiles given in Fig. 3a indicate that the T_{ODT} of SI2VP-13 lies somewhere between 210 and 220 °C and the temperature dependence of birefringence given in Fig. 3b indicates that the T_{ODT} of SI2VP-13 is about 215 °C, which is very close to the T_{ODT} determined from SAXS profiles. This value is also similar to that (about 210 °C) determined from the dynamic temperature sweep experiments under isochronal conditions at $\omega = 0.1$ rad/s (see Fig. 1a). Notice in Fig. 3a that the scattering peak appears at q^*, $\sqrt{3}q^*$,$\sqrt{4}q^*$, and $\sqrt{7}q^*$, and the intensity at q^* is much smaller than that at $\sqrt{3}q^*$ and $\sqrt{4}q^*$ Thus, the morphology of SI2VP-13 is not hexagonally packed cylindrical microdomains, but it has CSC microdomain structure. This is consistent with the TEM image given in Fig. 1b. Previously, Bailey et al. [38] also reported that the SAXS intensity at q^* was much smaller than that at $\sqrt{3}q^*$ and $\sqrt{4}\,q^*$ for the CSC microdomains in polystyrene-*block*-polyisoprene-*block*-poly(ethylene oxide) copolymer, consistent with the finding (Fig. 3a) from this study.

3.2. Dispersion characteristics of solution-blended organoclay nanocomposites based on disordered SI2VP-5

Fig. 4 gives XRD patterns of five nanocomposites based on SI2VP-5. It can be seen in Fig. 4 that the XRD patterns of (SI2VP-5)/MMT nanocomposite shows a broad reflection peak at approximately 7°, suggesting that this nanocomposite might have a poor dispersion of MMT aggregates, while the XRD patterns for four organoclay nanocomposites are featureless, suggesting that the organoclay aggregates might be dispersed well.

Fig. 5 shows TEM images of the following nanocomposites: (a) (SI2VP-5)/MMT, (b) (SI2VP-5)/Cloisite 15A®, (c) (SI2VP-5)/Cloisite 30B®, (d) (SI2VP-5)/Cloisite 10A®, and (e) (SI2VP-5)/Cloisite 25A®. We make the following observations from Fig. 5. (SI2VP-5)/MMT nanocomposite has very poor dispersion of MMT aggregates, while the four organoclay nanocomposites have a very high degree of dispersion (nearly exfoliated) of organoclay aggregates, confirming the speculation made above from the XRD patterns shown in Fig. 4. What is most interesting in Fig. 5 is that the degree of dispersion of the aggregates of all four organoclays (Cloisite 30B®, Cloisite 10A®,

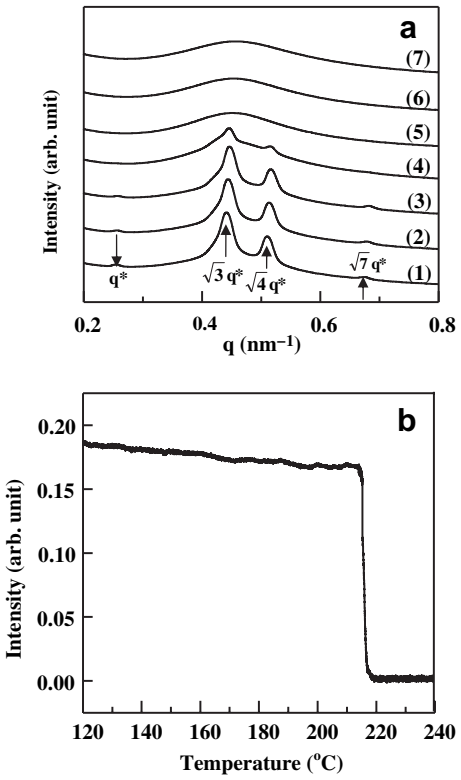

Fig. 3. (a) SAXS profiles of SI2VP-13 annealed at 180 °C for 48 h at various temperatures (°C); (1) 180, (2) 190, (3) 200, (4) 210, (5) 220, (6) 230, and (7) 240. (b) Temperature dependence of depolarized light scattering intensity of SI2VP-13 annealed at 180 °C for 48 h during heating at a rate of 0.5 °C/min.

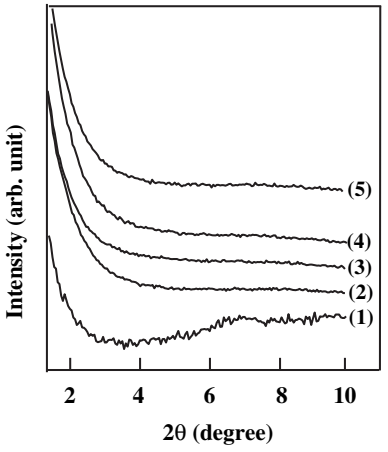

Fig. 4. XRD patterns of solution-blended nanocomposites based on SI2VP-5: (1) (SI2VP-5)/MMT, (2) (SI2VP-5)/Cloisite 15A®, (3) (SI2VP-5)/Cloisite 30B®, (4) (SI2VP-5)/Cloisite 10A®, and (5) (SI2VP-5)/Cloisite 25A®. All nanocomposite specimens were annealed at 90 °C for 48 h.

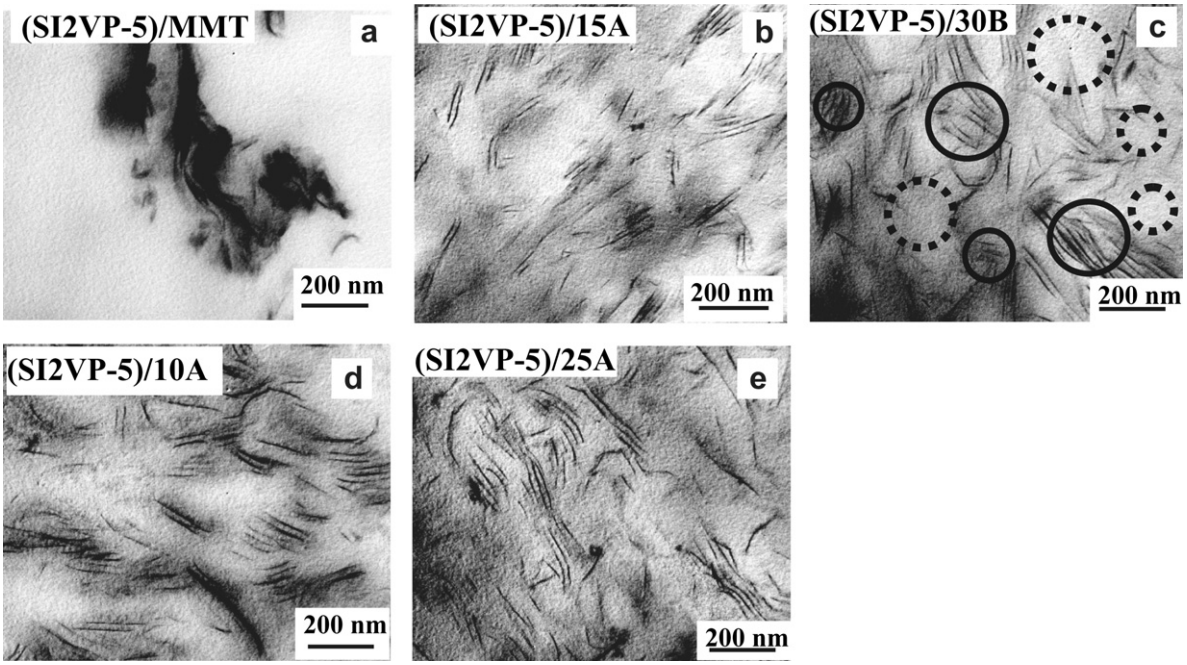

Fig. 5. TEM images of solution-blended nanocomposites based on SI2VP-5: (a) (SI2VP-5)/MMT, (b) (SI2VP-5)/Cloisite 15A®, (c) (SI2VP-5)/Cloisite 30B®, (d) (SI2VP-5)/Cloisite 10A®, and (e) (SI2VP-5)/Cloisite 25A®. All nanocomposite specimens were annealed at 90 °C for 48 h. Two distinct regions are shown in Fig. 5(c): one region encircled with the solid line where some organoclay platelets are regularly aligned along a specific direction and another region encircled with the dotted line where organoclay platelets are not discernible.

Cloisite 15A®, and Cloisite 25A®) is equally good, regardless of the differences in the chemical structures of the surfactants residing at the surface of the respective organoclays. Notice in Table 2 that all four surfactants residing at the surfaces of respective organoclays have quaternary ammonium chloride and thus N^+ ion. On the basis of our very recent investigation [26], we conclude that the very high degree of dispersion observed in the four organoclay nanocomposites, shown in Fig. 5, is attributable to the presence of ion–dipole interactions between the polar pyridine ring in the P2VP block of SI2VP-5 and the positively charged N^+ ion in the surfactant residing at the surface of each of the organoclays. Finally, notice in Fig. 5 that some clay platelets are regularly aligned along a specific direction in certain regions (for instance, the regions encircled with the solid line in Fig. 5c), while clay platelets are barely observed in other regions encircled with the dotted line in Fig. 5c. This observation is quite unusual for polymer nanocomposites with exfoliated clay platelets, because the exfoliated clay platelets are more uniformly dispersed throughout the entire sample.

In the past, for instance, Yoon et al. [12] reported on the preparation of organoclay nanocomposites based on polycarbonate (PC) and 12 different organoclays each having a surfactant having tallow or hydrogenated tallow and quaternary ammonium ion (N^+). What was common in the chemical structure of the surfactants employed by them was that all 12 surfactants contained quaternary ammonium ion (N^+) (given in Fig. 1 and Table 2 in ref [12]), which happened to be the same as those in the four surfactants employed in the present study (see Table 2). However, the findings between the two studies are quite different. Specifically, Yoon et al. [12] concluded that *none* of the 12 organoclay nanocomposites had exfoliation and the nanocomposites formed from a range of both intercalated tactoids having several platelets and sometimes large aggregates and collapsed clay particles as determined by TEM micrographs. A close look at the chemical structures of the 12 surfactants, employed in the study of Yoon et al. which resided at the surface of different organoclays, suggests to us that little or no strong attractive interactions would have existed with the PC matrix and thus no exfoliated nanocomposites would have been expected, as it turned out to be the case. As pointed out above, this was not the case in the present study, in which strong attractive interactions existed between the polar pyridine ring in the P2VP block of SI2VP-5 and the positively charged N^+ ion in the surfactant residing at the surface of each of the four organoclays employed. The above observations point out the importance of a judicious design (or choice) of a polymer matrix in the preparation of exfoliated organoclay nanocomposites.

Fig. 6 shows TEM images of (a) (SI2VP-5)/MMT nanocomposite annealed at 90 °C for 48 h, (b) (SI2VP-5)/Cloisite 15A® nanocomposite annealed at 90 °C for 48 h, (c) (SI2VP-5)/Cloisite 15A® nanocomposite annealed at 170 °C for 24 h, (d) (SI2VP-5)/Cloisite 30B® nanocomposite annealed at 90 °C for 48 h, and (e) (SI2VP-5)/Cloisite 30B® nanocomposite annealed at 170 °C for 24 h. Note in Fig. 6 that the polyisoprene (PI) phase of SI2VP-5 was stained with osmium tetroxide and thus the dark areas represent the PI phase and the bright areas represent the polystyrene (PS) phase. It is difficult to discern the P2VP phase in the TEM images, because the amount of P2VP block in the block copolymer is very small. The following observations are worth noting in Fig. 6. (SI2VP-5)/MMT nanocomposite (Fig. 6a) shows very large MMT aggregates suspended in the matrix of SI2VP-5 that is composed of disordered frozen concentration fluctuations, which were formed upon rapid quenching of the sample in ice water after annealing at 90 °C for 48 h. It should be remembered that SI2VP-5 is a homogeneous block copolymer (see Fig. 1). A close look at the TEM images of (SI2VP-5)/Cloisite 15A® and (SI2VP-5)/Cloisite 30B® nanocomposites in Fig. 6b–e reveals, that regardless of whether the specimens were annealed at 90 °C for 48 h or at 170 °C for 24 h, the stacks consisting of dark and bright stripes are observed in some areas (for instance, the regions encircled by the solid line in Fig. 6e). Note that these patterns are very similar to the layered structures that are often observed in a block copolymer having lamellar microdomains. This observation suggests that the chain conformation of SI2VP-5 chains in these regions would be different from

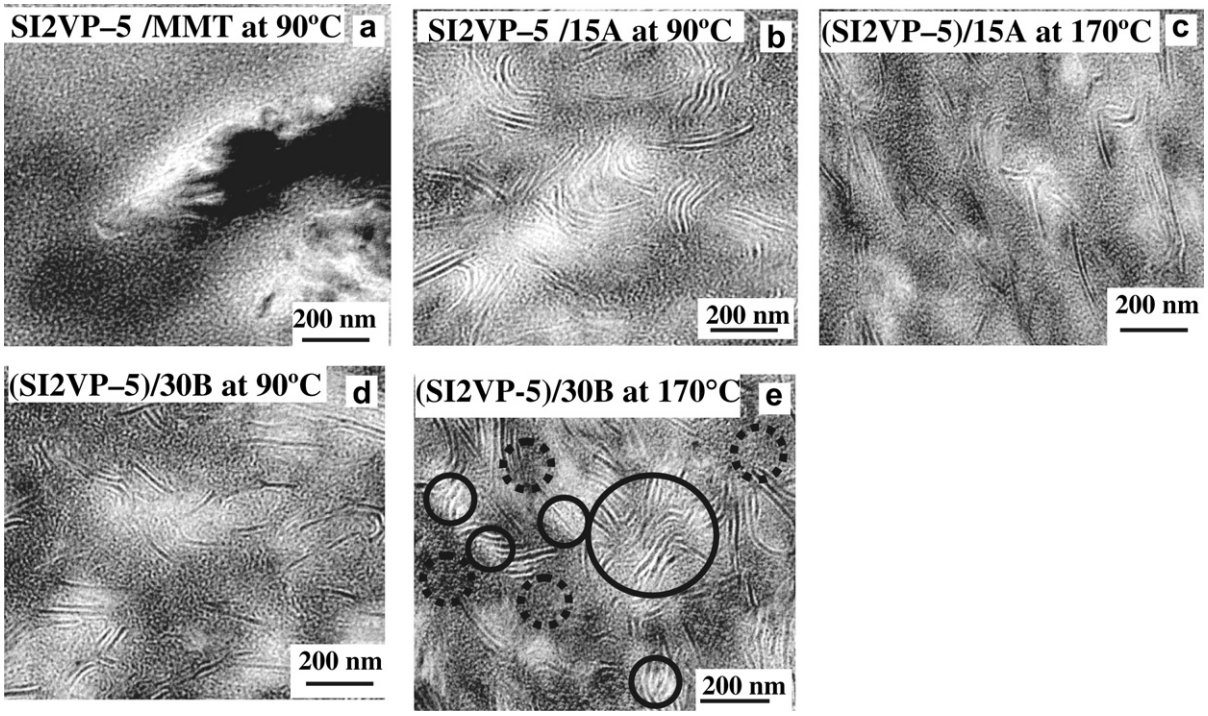

Fig. 6. TEM images of solution-blended nanocomposites based on SI2VP-5 subjected to different annealing conditions in which the PI phase of SI2VP-5 was stained with osmium tetroxide: (a) (SI2VP-5)/MMT annealed at 90 °C for 48 h, (b) (SI2VP-5)/Cloisite 15A® annealed at 90 °C for 48 h, (c) (SI2VP-5)/Cloisite 15A® annealed at 170 °C for 24 h, (d) (SI2VP-5)/Cloisite 30B® annealed at 90 °C for 48 h, and (e) (SI2VP-5)/Cloisite 30B® annealed at 170 °C for 24 h. Two distinct regions are shown in Fig. 6(e): one region encircled with the solid line where the stacks consisting of dark and bright stripes are observed and another encircled with the dotted line where only the disordered structures of SI2VP-5 are seen.

the homogeneous triblock copolymer SI2VP-5. Since only the presence of organoclay (Cloisite 15A® or Cloisite 30B®) could have changed the block copolymer chain conformation in these nanocomposites, it is very reasonable to speculate that organoclay platelets are present inside the regions encircled by the solid line. Although the TEM image alone does not provide the direct evidence of the presence of organoclay platelets in this region, the SAXS results presented below will support our speculation made above. However, other regions (encircled by the dotted line in Fig. 6e) do not show stacks of dark and bright stripes, but only disordered SI2VP-5 structure is seen. Interestingly, the distance between two dark stripes (or two bright stripes) is very similar to that between two neighboring organoclay platelets that can be seen in Fig. 5b–e. Thus, the two different regions shown in Fig. 5c might be correlated with those shown in Fig. 6e. Since the TEM images given in Fig. 6 did not provide conclusive evidence as to whether the added organoclay had induced microphase separation in the homogeneous SI2VP-5, we conducted a series of SAXS experiments to resolve this issue.

Fig. 7a gives SAXS profiles at various temperatures during heating from 100 to 200 °C for an (SI2VP-5)/Cloisite 30B® nanocomposite specimen, which was annealed at 180 °C for 48 h. It is interesting to observe in Fig. 7a that the scattering peaks with Bragg spacings with the following ratios, 1:2:3:4:5, representing an arrangement of alternating layers of lamellae, persist as the temperature of the specimen is increased from 100 to 200 °C although the SAXS peaks are not very sharp. Also, the position of the first order SAXS peak is about 0.26 nm^{-1} (thus, the *d*-spacing is about 24 nm), which is distinctly smaller than that of the correlation hole peak (about 0.42 nm^{-1}) of neat SI2VP-5, as shown in Fig. 2a. Note that the *d*-spacing in Fig. 7a is close to the distance between two neighboring bright stripes (the PS phase) in the TEM images shown in Fig. 6b–e. Furthermore, it is also close to the distance between two parallel stacks of organoclay platelets in the TEM images shown in Fig. 5b–e. Another interesting observation in Fig. 7a is that the scattering peak at $2q^*$ becomes sharper (not broader) with increasing temperature, which is quite different from neat block copolymers where the SAXS peak becomes broader with increasing temperature (see Fig. 2a for disordered SI2VP-5 and Fig. 3a for lamella-forming SI2VP-13).

To explain the SAXS profiles given in Fig. 7a as well as the TEM images in Figs. 5b–e and 6b–e, we consider that the (SI2VP-5)/Cloisite 30B® nanocomposite has two distinct regions, region I and region II, as schematically shown in Fig. 8. Note that region I is occupied only by disordered SI2VP-5 chains, and region II consists of disordered SI2VP-5 chains (the bright areas) and Cloisite 30B® platelets (the thin dark lines), having attractive ion–dipole interactions between the pyridine ring in the P2VP block and the positively charged N^+ ion in the surfactant residing at the surface of Cloisite 30B®. We postulate further that when the P2VP chains in SI2VP-5 interact with the N^+ ion, they would be located near the surface of the organoclay. Under this scenario we expect that the aggregates of organoclay platelets could be exfoliated, even when a small number of P2VP chains is located near the surface of the organoclay surface. Due to the chain architecture of SI2VP-5, the PI chains would be located next to the P2VP chains, and the PS block chains are located next to the PI chains. Then, the chain conformation of SI2VP-5 in region II can be regarded as being tethered chains on the surface of Cloisite 30B®. When the number density of tethered chains exceeds a certain critical value (although its exact value is not estimated here), two (or more) Cloisite 30B® platelets could be rearranged in such a way that they form parallel platelets, inside of which the PI and PS blocks have their own microdomains to reduce the enthalpic penalty between the two blocks. However, the perfectly parallel alignment of the organoclay platelets would

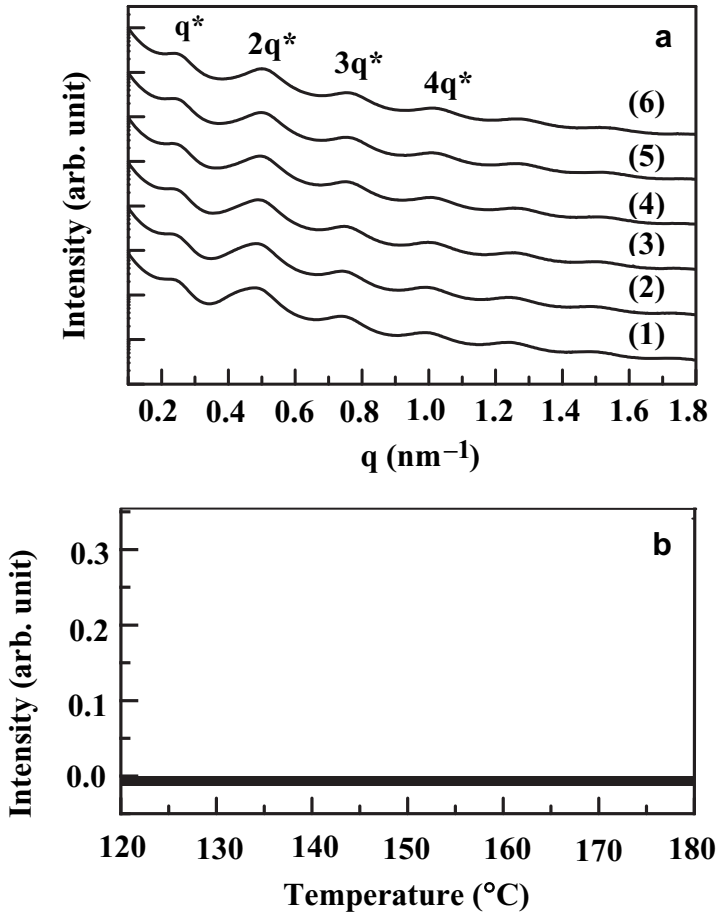

Fig. 7. (a) SAXS profiles of solution-blended (SI2VP-5)/Cloisite 30B® nanocomposite, which was annealed at 180 °C for 48 h, at various temperatures (°C): (1) 100, (2) 120, (3) 140, (4) 160, (5) 180, and (6) 200. (b) Temperature dependence of depolarized light scattering for solution-blended (SI2VP-5)/Cloisite 30B® nanocomposite at temperatures ranging from 120 to 180 °C.

not be possible, because the number of tethered chains at the surface of each organoclay platelet would be different. The most probable conformation of SI2VP-5 chains within region II shown in Fig. 8 would be lamellar microdomains, because the volume fractions of the PI and PS blocks are very close to each other (see Table 1).

Thus, the SAXS profiles of the (SI2VP-5)/Cloisite 30B® nanocomposite given in Fig. 7a might have been affected by the presence of the two distinct regions, region I and region II. It should be remembered that the correlation hole peak appearing at about 0.42 nm^{-1} (see Fig. 2a) originated from the disordered SI2VP-5 chains (region I) and another peak (q^*) appearing at about 0.26 nm^{-1} originated from the aligned Cloisite 30B® platelets, inside of which organoclay-induced alternating layers of PI and PS microdomains exist (region II). Since the correlation hole peak position (at about 0.42 nm^{-1}) is not much different from the peak position $2q^*$ (at about 0.52 nm^{-1}), the SAXS profile in Fig. 7a appearing at values of q between 0.4 and 0.6 nm^{-1} might be attributable to the combination of these two peaks. Thus, at lower temperatures (say at 100 °C) the SAXS profile of the (SI2VP-5)/Cloisite 30B® nanocomposite shows a broad peak. But, this SAXS peak becomes sharper with increasing temperature, because the contribution of the correlation peak to the SAXS profile becomes negligibly small with increasing temperature (see Fig. 2a). On the other hand, at higher temperatures, only the $2q^*$ peak originating from the presence of the aligned Cloisite 30B® platelets contributes to the SAXS profile.

The reason why the d-spacing (24 nm, which was obtained from the first peak position $q^* = 0.26$ nm^{-1}) of the (SI2VP-5)/Cloisite 30B® nanocomposite given in Fig. 7a is distinctly larger than that (15 nm, corresponding to $q = 0.42$ nm^{-1}) of the correlation hole peak of neat SI2VP-5 given in Fig. 2a is as follows. The readers are reminded that SI2VP-5 chains are postulated to form alternating layers of lamellar microdomains inside two neighboring Cloisite 30B® platelets.

Since the sequence of the lamellar microdomains across the Cloisite 30B® platelet is P2VP/PI/PS/PS/PI/P2VP (see the right panel of Fig. 8), the distance between two neighboring Cloisite 30B® platelets would be close to the size of the lamellar microdomains of SI2VP-5 chains. According to Hashimoto et al. [39], the d-spacing of the lamellar microdomain for an SI diblock copolymer having a number-average molecular weight (M_n) of 9170 for each block is estimated to be about 17 nm. Since SI2VP-5 has an additional P2VP block having an M_n of 960, the d-spacing (about 24 nm) obtained from the SAXS profile seems reasonable when the layer of P2VP block is included.

Based on the above arguments and SAXS results given in Fig. 7a, the regions encircled with the dotted line shown in Figs. 5c and 6e correspond to region I given in Fig. 8, whereas the regions encircled with the solid line, shown in Figs. 5c and 6e, correspond to region II shown in Fig. 8.

Although lamellar microdomain structures probably exist between two neighboring Cloisite 30B® platelets in the (SI2VP-5)/Cloisite 30B® nanocomposite, they are completely different from

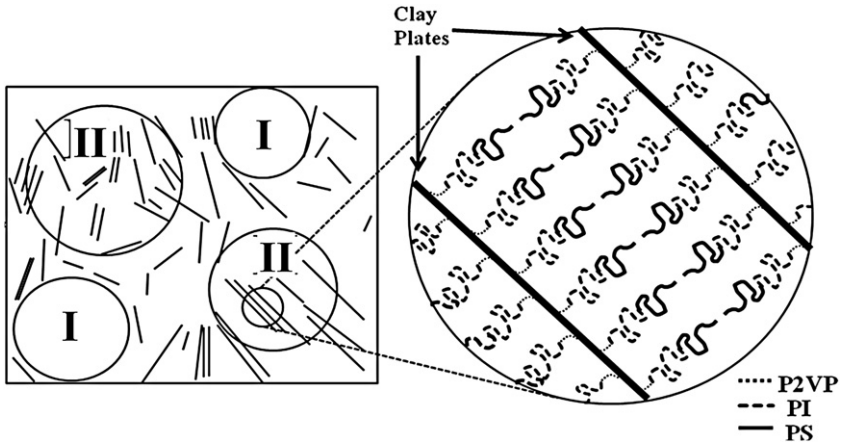

Fig. 8. Schematic describing the presence of two regions (I and II) in the (SI2VP-5)/organoclay nanocomposites, in which region I has only disordered SI2VP-5 chains and region II has aligned organoclay platelets, inside of which SI2VP-5 chains form lamellar microdomain structures. The right-side panel describes the chain conformation of lamella-forming SI2VP-5 chains residing between two neighboring organoclay platelets denoted by thick sticks. The alternating layers of lamella-forming microdomains have the following sequence, P2VP/PI/PS/PS/PI/P2VP.

the lamellar microdomain structures observed in compositionally symmetric AB-type diblock and ABA-type triblock copolymers. Namely, in the latter situation the alternating layers of lamellar microdomains are repeated throughout the entire sample, while in the former situation only several stacks exist in the nanocomposites under consideration here. Above, we have speculated that in the former situation lamellar microdomains probably are formed between two neighboring Cloisite 30B® platelets. These lamellar microdomains could not be detected by birefringence experiments. Thus, the (SI2VP-5)/Cloisite 30B® nanocomposite did not show any static birefringence over the entire range of temperatures tested, as shown in Fig. 7b.

It should be mentioned that the SAXS profile of the (SI2VP-5)/Cloisite 15A® nanocomposite showed the scattering peaks at positions having the ratios, 1:2:3:4:5, which are essentially the same as those for the (SI2VP-5)/Cloisite 30B® nanocomposite, the profiles of which are not shown here due to space limitations. This nanocomposite also has a region where Cloisite 15A® platelets are aligned along a specific direction, as shown in the TEM images given in Figs. 5 and 6.

3.3. Dispersion characteristics of solution-blended organoclay nanocomposites based on microphase-separated, low-molecular-weight SI2VP-13

Fig. 9 gives XRD patterns of four nanocomposites based on SI2VP-13. It should be remembered that SI2VP-13 is a microphase-separated block copolymer having CSC microdomains (see the TEM image given in Fig. 1b and SAXS profiles given in Fig. 3a). It can be seen in Fig. 9 that the XRD patterns of (SI2VP-13)/MMT nanocomposite show a broad reflection peak at approximately 8°, suggesting that this nanocomposite might have a poor dispersion of MMT aggregates, while the XRD patterns for the three organoclay nanocomposites are featureless, suggesting that the organoclay aggregates might be dispersed well.

Fig. 10 shows TEM images of (a) (SI2VP-13)/MMT nanocomposite, (b) (SI2VP-13)/Cloisite 15A® nanocomposite, (c) (SI2VP-13)/Cloisite 30B® nanocomposite, and (d) (SI2VP-13)/Cloisite 30B®-10 nanocomposite in which Cloisite 30B®-10 denotes 10 wt% Cloisite 30B® in the nanocomposite, whereas the other three nanocomposites have 5 wt% MMT, Cloisite 15A® or Cloisite 30B®. The following observations are worth noting from Fig. 10. The aggregates of MMT are hardly dispersed in the matrix of SI2VP-13, while the aggregates of both Cloisite 15A® and Cloisite 30B® are well dispersed in the matrix of SI2VP-13 although the state of dispersion in the (SI2VP-13)/Cloisite 15A® nanocomposite does not appear to be as good as that in the (SI2VP-13)/Cloisite 30B® nanocomposite, confirming the speculation made above from the XRD patterns shown in Fig. 9. Again, it is interesting to observe in Fig. 10 that the difference in chemical structure of the surfactants, MT2EtOH residing at the surface of Cloisite 30B® and 2M2HT residing at the surface of Cloisite 15A®, has little effect on the dispersion characteristics of the organoclay aggregates. This observation is very similar to that made above for the nanocomposites based on homogeneous SI2VP-5 (see Fig. 5). Thus, the conclusion drawn above for the organoclay nanocomposites based on SI2VP-5 also applies to the nanocomposites based on SI2VP-13.

Fig. 11 shows TEM images of the following nanocomposites: (a) (SI2VP-13)/MMT, (b) (SI2VP-13)/Cloisite 15A®, and (c) (SI2VP-13)/Cloisite 30B®, all annealed at 210 °C for 24 h. Notice in Fig. 11 that the dark areas represent the PI phase, which was stained with osmium tetroxide, and the bright areas represent the PS phase. The following observations are worth noting in Fig. 11. In Fig. 11a we

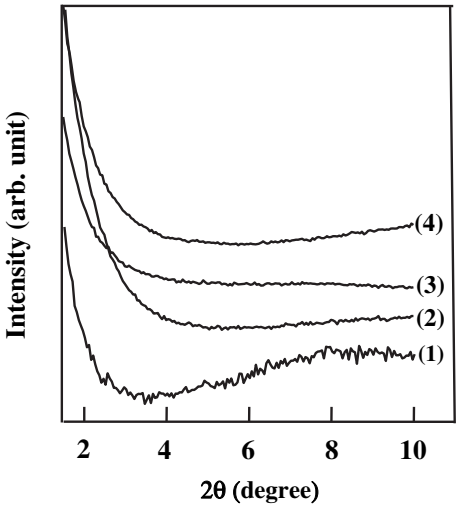

Fig. 9. XRD patterns for solution-blended nanocomposites based on SI2VP-13: (1) (SI2VP-13)/MMT, (2) (SI2VP-13)/Cloisite 15A®, (3) (SI2VP-13)/Cloisite 30B®, and (4) (SI2VP-13)/Cloisite 30B®-10. All nanocomposite specimens were annealed at 120 °C for 48 h.

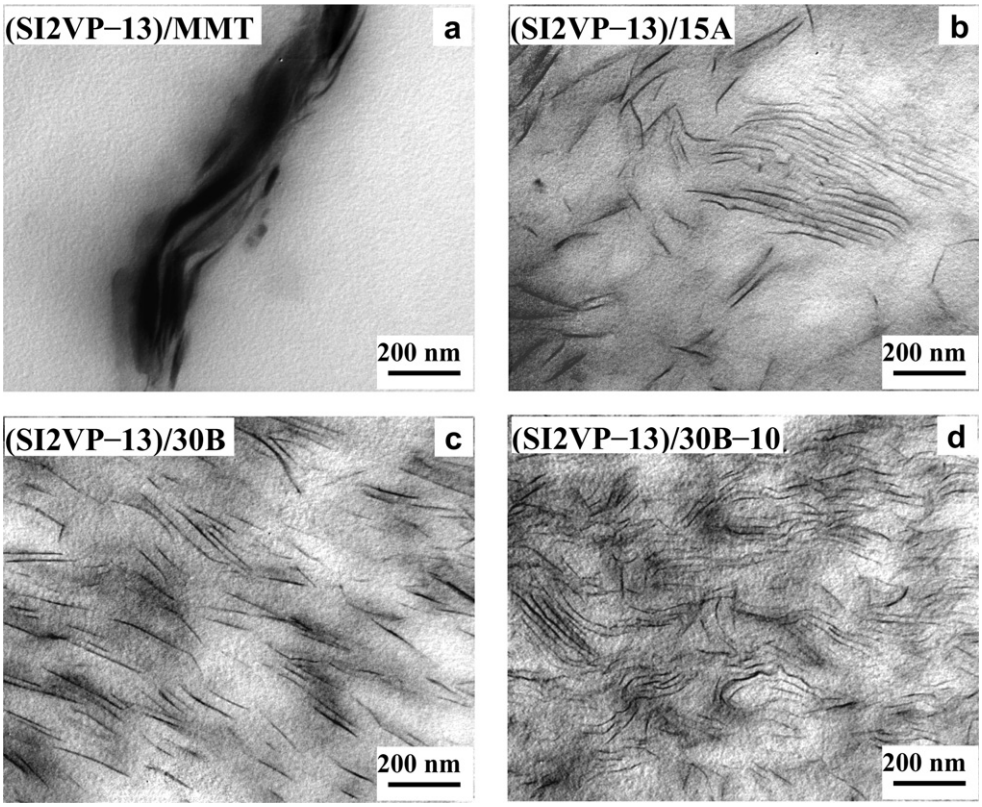

Fig. 10. TEM images of solution-blended nanocomposites based on SI2VP-13: (a) (SI2VP-13)/MMT, (b) (SI2VP-13)/Cloisite 15A®, (c) (SI2VP-13)/Cloisite 30B®, and (d) (SI2VP-13)/Cloisite 30B®-10, where the block copolymer was not stained. All nanocomposite specimens were annealed at 120 °C for 48 h.

observe that after quenching in ice water from 210 °C (which is very close to the T_{ODT} of neat SI2VP-13), the TEM image of (SI2VP-13)/MMT nanocomposite shows very large MMT aggregates suspended in the SI2VP-13 matrix and the morphology of SI2VP-13 in Fig. 11a looks very similar to that (disordered concentration fluctuations) shown in Fig. 6a for the (SI2VP-5)/MMT nanocomposite. It is clear that there is no compatibility between MMT and SI2VP-13. It should be remembered that neat SI2VP-13 has CSC microdomains and a T_{ODT} of approximately 210 °C (see Fig. 3). In Fig. 11b and c we observe that, regardless of the differences in the chemical structures of the surfactants, MT2EtOH and 2M2HT, both (SI2VP-13)/Cloisite 15A® and (SI2VP-13)/Cloisite 30B® nanocomposites have virtually the same degree of good dispersion of organoclay aggregates. It can be seen in the enlarged section of Fig. 11c that the exfoliated organoclay platelets are located near the PI phase, and CSC microdomains are seen outside the layer of (SI2VP-13)/Cloisite 30B® nanocomposite. The details of the chain conformation will be discussed after the presentation of SAXS profiles.

Fig. 12 gives SAXS profiles at various temperatures of (a) (SI2VP-13)/Cloisite 15A® and (b) (SI2VP-13)/Cloisite 30B® nanocomposites, both annealed at 180 °C for 48 h. It should be remembered that neat SI2VP-13 has CSC microdomains at 180 °C (see Fig. 3a). It can be seen in Fig. 12 that the scattering peaks are observed at q^* ratios of 1:2:3:4. Based on Figs. 10–12, we speculate that the nanocomposites based on SI2VP-13 have two different regions, region I and region II, as schematically shown in Fig. 13. Referring to Fig. 13, region I is occupied only by SI2VP-13 chains and region II consists of microphase-separated SI2VP-13 and exfoliated organoclay platelets (Cloisite 30B® or Cloisite 15A®). It should be remembered that SI2VP-13 has CSC microdomain structures at temperatures below T_{ODT}, but becomes a disordered state at temperatures above T_{ODT} (see Fig. 3). Region II in Fig. 13 is affected by the favorable interaction between the pyridine ring in the P2VP block and positively charged N^+ ion in the surfactant residing at the surface of the of the organic clay. In region II the aggregates of organoclay (Cloisite 30B® or Cloisite 15A®) are exfoliated with increasing number density of P2VP chains on the surface of the organoclay platelets. Then, the chain conformation of SI2VP-13 in region II should be quite different from that in neat SI2VP-13. Namely, the P2VP block in neat SI2VP-13 forms the core of the CSC microdomain structure (see Fig. 1b), because the P2VP phase has the smallest volume fraction in SI2VP-13 (see Table 1). However, due to the strong attractive interaction with the N^+ ion on the surface of the organoclay (Cloisite 30B® or Cloisite 15A®), the P2VP phase in SI2VP-13 is expected to cover the surface of the organoclay platelets. Under such a circumstance, the P2VP phase would no longer be able to form the core of the CSC microdomain structure. Instead, the P2VP phase would form a layer, resulting in both PI and PS blocks that form their own lamellar microdomains. But, a perfect parallel alignment of organoclay platelets would not be possible, because the number of chains tethered to each organoclay platelet would vary in a given nanocomposite specimen. However, some of the organoclay platelets could be aligned along a specific direction, as shown in the TEM images given in Figs. 10 and 11. The sequence of the layers for SI2VP-13 chains across the organoclay platelet is expected to be PVP/PI/PS/PS/PI/P2VP, as schematically shown on the right-side panel of Fig. 13. This speculation is confirmed by the enlarged TEM image given in Fig. 11c, in which the organoclay platelet lies within the alternating layers of PS and PI blocks. It is also seen in Fig. 12a that there exists another peak (at about 0.48 nm^{-1}) near the scattering peak at $2q^*$ (about 0.43 nm^{-1}) at lower temperatures for (SI2VP-13)/Cloisite 15A® nanocomposite. Since the scattering peak at about 0.51 nm^{-1} corresponds to $\sqrt{4}q^*$of the CSC microdomain structure, this

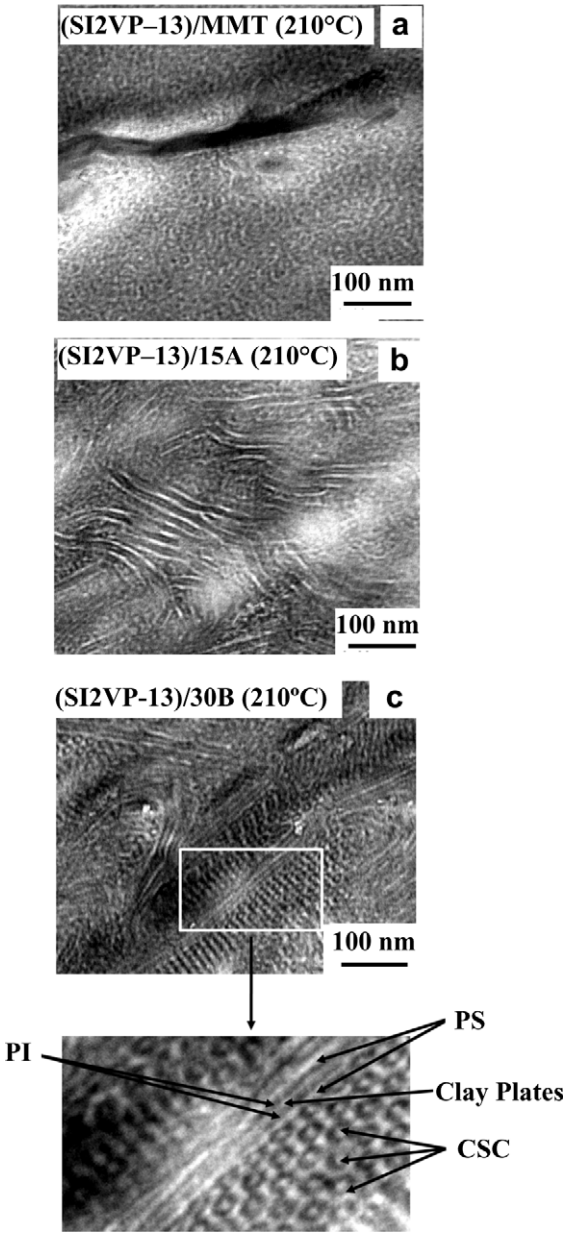

Fig. 11. TEM images of solution-blended nanocomposites based on SI2VP-13: (a) (SI2VP-13)/MMT, (b) (SI2VP-13)/Cloisite 15A®, and (c) (SI2VP-13)/Cloisite 30B®, all annealed at 210 °C for 24 h. Notice that the dark areas represent the PI phase which was stained with osmium tetroxide, the bright areas represent the PS phase, and it is very difficult to identify the P2VP phase in the TEM images. Notice in the enlarged section of Fig. 11c that the exfoliated organoclay platelets are located near the PI phase, and CSC microdomains are seen outside the layer of (SI2VP-13)/Cloisite 30B® nanocomposite.

observation also confirms that two different regions (regions I and II in Fig. 13) contribute to the SAXS profiles at low temperatures (say at 120 °C). However, the scattering peak for the CSC microdomain structure should disappear at higher temperatures (above the T_{ODT} of SI2VP-13).

The *d*-spacing of (SI2VP-13)/Cloisite 15A® and (SI2VP-13)/Cloisite 30B® nanocomposites is 29 nm, which is obtained from the first scattering peak at $q^* = 0.215$ nm^{-1}. This value is 1.2 times larger than that (24 nm) of the nanocomposite based on SI2VP-5. The slight increase observed in the *d*-spacing is due to the fact that the layer thickness corresponding to the P2VP block in SI2VP-13 is expected to be larger than that corresponding to the P2VP block in

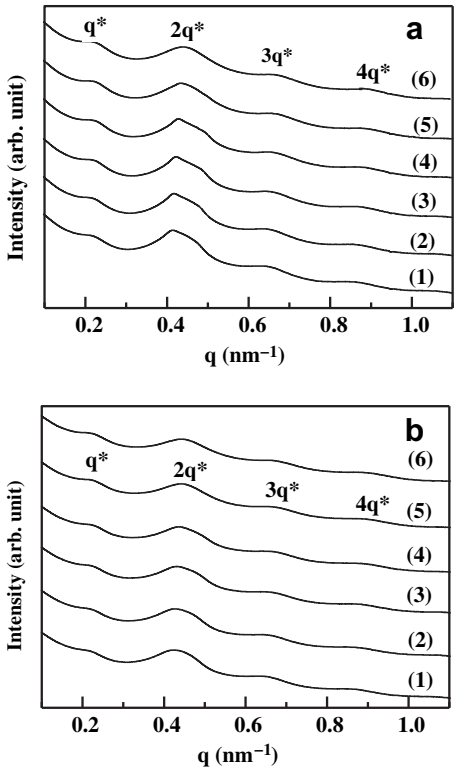

Fig. 12. SAXS profiles of (a) solution-blended (SI2VP-13)/Cloisite 15A® nanocomposite annealed at 180 °C for 48 h, and (b) solution-blended (SI2VP-13)/Cloisite 30B® nanocomposite annealed at 180 °C for 48 h at various temperatures (°C): (1) 120, (2) 140, (3) 160, (4) 180, (5) 200, and (6) 220.

SI2VP-5, because the molecular weight (and the volume fraction) of the P2VP block in SI2VP-13 is larger than that in SI2VP-5 (see Table 1). Finally, in Fig. 12b the scattering peak at about 0.48 nm^{-1} is not discernible even at low temperatures (say at 120 °C) for the (SI2VP-13)/Cloisite 30B® nanocomposite, which is different from the case for the SI2VP-13/Cloisite 15A® nanocomposite (compare Fig. 12a with Fig. 12b). This observation suggests that the region I for the (SI2VP-13)/Cloisite 30B® nanocomposite is smaller than that for the (SI2VP-13)/Cloisite 15A® nanocomposite.

3.4. Dispersion characteristics of melt-blended nanocomposites based on microphase-separated low-molecular-weight SI2VP-13

Fig. 14 shows XRD patterns of (SI2VP-13)/Cloisite 30B® nanocomposites prepared by melt blending at extruder barrel temperatures of 160 and 200 °C. We observe from Fig. 14 that the XRD patterns show no reflection peak for both nanocomposites suggesting that the organoclay aggregates might have been well dispersed, regardless of the temperatures at which the nanocomposites were prepared by melt blending. Fig. 15 gives TEM images of (SI2VP-13)/Cloisite 30B® nanocomposites prepared by melt blending at extruder barrel temperatures of 160 and 200 °C, in which the TEM images on the left-side panel were obtained without staining the block copolymer and the TEM images on the right-side panel were obtained with staining the PI phase using osmium tetroxide. In Fig. 15 we observe a very high degree of dispersion (near exfoliation) of the aggregates of organoclay Cloisite 30B® in the nanocomposites. Comparison of Fig. 15 with Figs. 10 and 11 reveals that there are little differences in the dispersion characteristics of (SI2VP-13)/Cloisite 30B® nanocomposites whether they were prepared by melt blending at 160 and 200 °C or

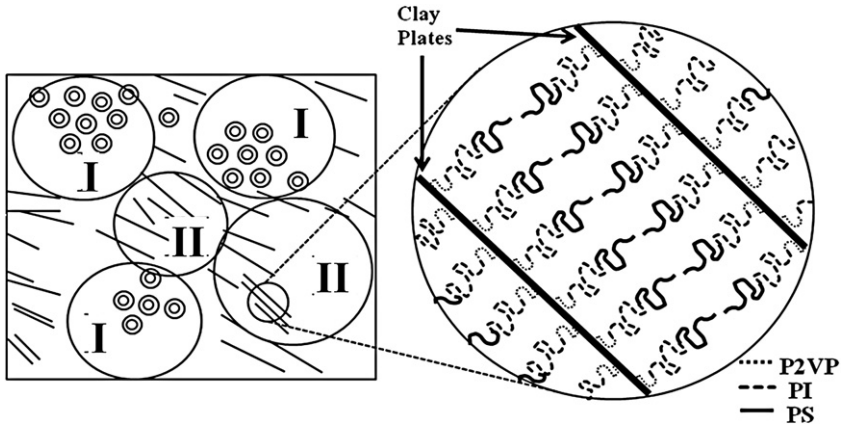

Fig. 13. Schematic describing the presence of two regions (I and II) in the (SI2VP-13)/organoclay nanocomposites, in which region I has only SI2VP-13 having CSC microdomain structures and region II has aligned organoclay platelets, inside of which SI2VP-13 chains form lamellar microdomain structures. The right-side panel describes the chain conformation of lamella-forming SI2VP-13 chains residing between two neighboring organoclay platelets denoted by thick sticks. The alternating layers of lamella-forming microdomains have the following sequence, P2VP/PI/PS/PS/PI/P2VP.

by solution blending. It should be mentioned that the SI2VP-13 triblock copolymer, which was employed to prepare the exfoliated nanocomposites the results of which are summarized in Figs. 14 and 15, had simply been dried at 120 °C for 48 h (i.e., the SI2VP-13 triblock copolymer was not annealed at elevated temperatures). We learned from isochronal dynamic temperature sweep experiment (not presented here for the reason of limited space) that the unannealed SI2VP-13 triblock copolymer had a T_{ODT} of about 190 °C. This information is relevant to the interpretation of the morphology evolution of the exfoliated nanocomposites during the isochronal dynamic temperature sweep experiment summarized below.

Fig. 16 describes variations of dynamic storage modulus (G') with temperature for: (▼) a specimen that was melt-blended at 160 °C for 6 min and (▲) a specimen that was melt-blended at 200 °C for 6 min. Also given in Fig. 16 are variations of G' with temperature for: (○) neat SI2VP-13 (□) solution-blended (SI2VP-13)/Cloisite 30B® nanocomposite, which had simply been dried at 120 °C for 48 h. It is seen in Fig. 16 that values of G' of nanocomposites prepared by melt blending at 160 or 200 °C for 6 min in a twin-screw mini-compounder go through a minimum at about 180 °C, indicating that after having been subjected to melt blending

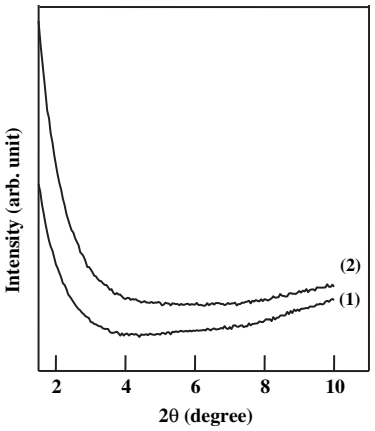

Fig. 14. XRD patterns of (SI2VP-13)/Cloisite 30B® nanocomposites which were prepared by melt blending for 6 min in a twin-screw mini-compounder at a screw speed of 180 rpm at two different extruder barrel temperatures: (1) 160 °C and (2) 200 °C.

the T_{ODT} of SI2VP-13 matrix in the exfoliated nanocomposites has decreased about 10 °C from 190 °C for unannealed, neat SI2VP-13. From the above observations we conclude that shearing motion inside the twin-screw mini-compounder played a significant role in disrupting the microdomains of SI2VP-13 in the nanocomposite and thus decreasing its T_{ODT} by 10 °C while being melt-blended at the extruder barrel temperature of 160 or 200 °C for 6 min. It is well established in the literature [40] that annealing of a microphase-separated block copolymer affects its T_{ODT}.

An interesting aspect of Fig. 16 is that values of G' of both melt-blended nanocomposite samples increase very rapidly after passing through a minimum at about 180 °C, a signature of T_{ODT}. This observation is quite unusual in that values of G' decrease steadily with increasing temperature for all flexible homopolymers and random copolymers, and disordered block copolymers. A further interesting observation that can be made from Fig. 16 is that values of G' of the solution-blended specimen are much larger than those of the melt-blended specimen and they decrease steadily with increasing temperature from 120 to 220 °C without going through a minimum, behavior quite different from the temperature dependence of G' of melt-blended specimens. Notice in Fig. 16 that values of G' merge to about 6000 Pa at about 220 °C, regardless of whether the nanocomposite was prepared by melting blending at two different extruder barrel temperatures or prepared by solution blending. The temperature dependence of G' of melt-blended nanocomposites observed from Fig. 16 is quite unusual and unique. To our knowledge, no such experimental observations have ever been reported in the literature.

In order to investigate whether melt blending of (SI2VP-13)/Cloisite 30B® nanocomposite in the twin-screw mini-compounder might have degraded or broken down SI2VP-13 molecules, we measured the molecular weight of SI2VP-13, via gel permeation chromatography (GPC), before and after melt blending. For the GPC measurements, we first dissolved SI2VP-13 by placing a nanocomposite sample in THF and then recovered the polymer by centrifuge followed by drying. Fig. 17 gives GPC traces of (a) neat SI2VP-13, (b) SI2VP-13 after the nanocomposite was prepared by melt blending at an extruder barrel temperature of 160 °C for 6 min, and (c) SI2VP-13 after the nanocomposite was prepared by melt blending at an extruder barrel temperature of 200 °C for 6 min. In Fig. 17 we cannot discern any differences in the GPC traces of the three SI2VP-13 specimens, leading us to conclude that the very unusual temperature dependence of G' of melt-blended

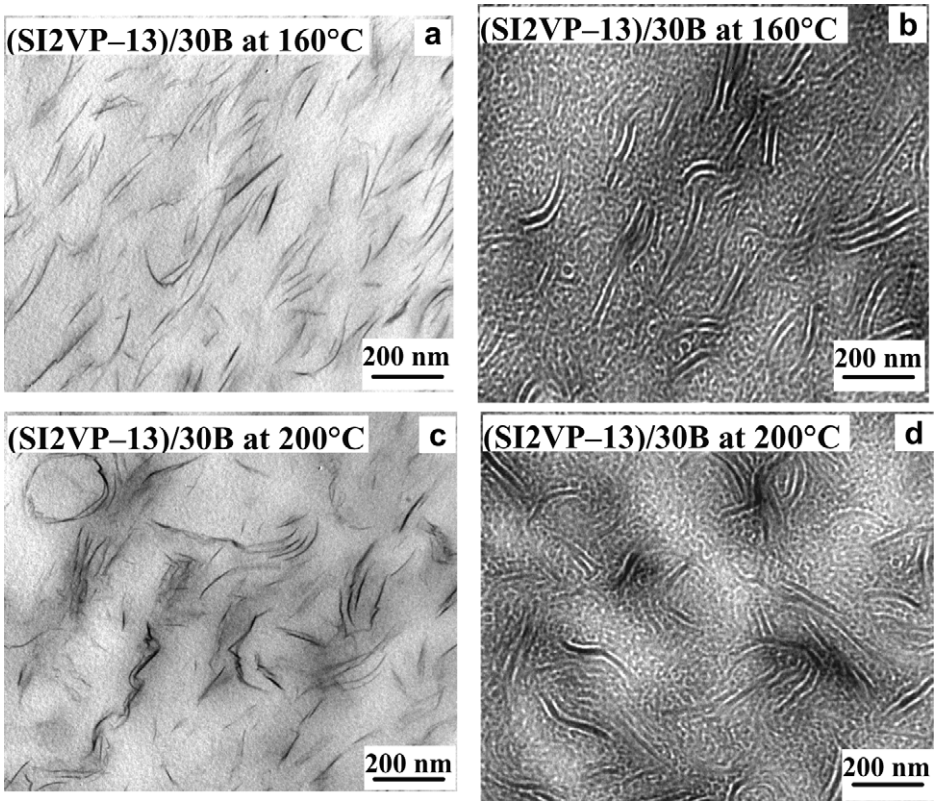

Fig. 15. TEM images (a) without staining and (b) with staining of (SI2VP-13)/Cloisite 30B® nanocomposites which were prepared by melt blending at an extruder barrel temperature of 160 °C for 6 min in a twin-screw mini-compounder at a screw speed of 180 rpm, and TEM images (c) without staining and (d) with staining of (SI2VP-13)/Cloisite 30B® nanocomposites which were prepared by melt blending at an extruder barrel temperature of 200 °C for 6 min in a twin-screw mini-compounder at a screw speed of 180 rpm.

(SI2VP-13)/Cloisite 30B® nanocomposite observed in Fig. 16 is not related to any possible molecular degradation of SI2VP-13 during compounding in the twin-screw mini-compounder.

In order to explain the interesting experimental observations made from Fig. 16, we conducted SAXS experiments, which enabled us to understand the origin of the rapid increase in G' of the melt-blended specimens after going through a minimum. Fig. 18a gives SAXS profiles at various temperatures during heating from 120 to 220 °C for (SI2VP-13)/Cloisite 30B® nanocomposite specimens which were prepared by melt blending at an extruder barrel temperature of 160 °C for 6 min. The following observations are worth noting in Fig. 18a. (1) In the SAXS profiles at 120 and 140 °C each show a broad, single scattering peak. (2) Two separate scattering peaks are observed as the temperature is increased to 160 °C and these peaks correspond to the CSC microdomains of SI2VP-13. (3) The SAXS profiles at temperatures above 200 °C show the scattering peaks at q^* ratios of 1: 2: 3: 4, although the peaks at q^*, $3q^*$, and $4q^*$ are very weak. Interestingly, these peaks were not observed at temperatures below 180 °C, which is quite different from the SAXS profiles for the (SI2VP-13)/Cloisite 30B® nanocomposite prepared by solution blending (see Fig. 12a).

The difference in SAXS profiles between melt-blended and solution-blended samples can be explained by the different volumes of regions I and II shown schematically in Fig. 13. Namely, the volume of region II, where organoclay platelets are aligned along a specific direction, in the melt-blended sample is expected to be smaller than that in the solution-blended sample. The reason is that the reorganization of PS and PI chains into their own lamellar microdomains between two neighboring organoclay platelets is limited by the small number of the tethered block chains due to the short mixing period of 6 min inside the twin-screw mini-compounder. However, even during this short mixing period, it is possible that the aggregates of organoclay could be well dispersed in the SI2VP-13 matrix during melt blending owing to the strong attractive interactions between the pyridine ring in P2VP blocks of SI2VP-13 and the positively charged N^+ ion residing at the surface of organoclay Cloisite 30B®. Further, well-developed CSC microdomain structures, where two separate scattering peaks are clearly

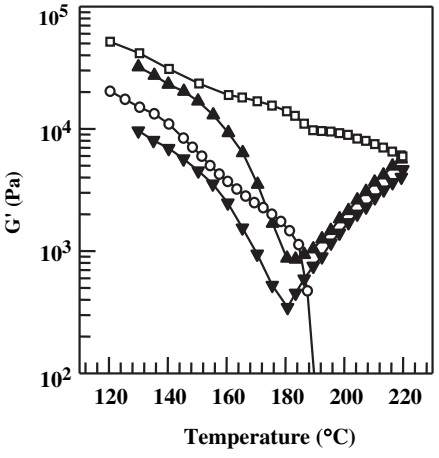

Fig. 16. Variations of dynamic storage modulus G' with temperature during isochronal temperature sweep experiments at an angular frequency of 0.1 rad/s for: (▼) (SI2VP-13)/Cloisite 30B® nanocomposite, which was prepared by melt blending at the extruder barrel temperature of 160 °C for 6 min in a twin-screw mini-compounder at a screw speed of 180 rpm, (▲) (SI2VP-13)/Cloisite 30B® nanocomposite, which was prepared by melt blending at an extruder barrel temperature of 200 °C for 6 min in a twin-screw mini-compounder at a screw speed of 180 rpm, (○) neat SI2VP-13, and (□) solution-blended (SI2VP-13)/Cloisite 30B® nanocomposite. Both neat SI2VP-13 and nanocomposite specimens were annealed at 120 °C for 48 h.

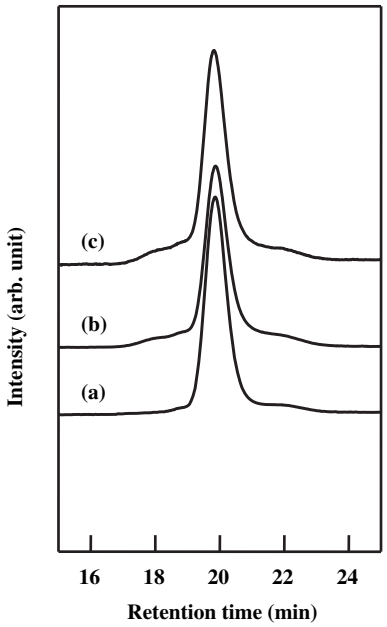

Fig. 17. GPC traces of (a) neat SI2VP-13, (b) SI2VP-13 after melt blending with Cloisite 30B® at an extruder barrel temperature of 160 °C for 6 min in a twin-screw mini-compounder at a screw speed of 180 rpm and (c) SI2VP-13 after melt blending with Cloisite 30B® at an extruder barrel temperature of 200 °C for 6 min in a twin-screw mini-compounder at a screw speed of 180 rpm.

observed at values of q ranging from 0.4 to 0.6 nm^{-1} (see Fig. 3a), could not be formed in region I in the melt-blended sample. For this reason, the SAXS profiles at 120 and 140 °C given in Fig. 18 do not exhibit the two separate scattering peaks in this range of q (from 0.4 to 0.6 nm^{-1}). In addition, in the SAXS profiles given in Fig. 18 the scattering peaks appearing at q^* ratios of 1: 2: 3: 4 are barely observed at 120 and 140 °C. With increasing temperature to about 160 °C, the CSC microdomain structure could be well developed in region I, which would give rise to two separate SAXS peaks at q values ranging from 0.4 to 0.6 nm^{-1}. However, the amount of aligned organoclay platelets along a specific direction (or the volume of region II) is still small due to the relatively small number of tethered chains; thus the SAXS profiles do not show the scattering peaks at q^* ratios of 1: 2: 3: 4 at 160 °C.

However, with sufficiently high temperature which is close to or higher than the T_{ODT} (about 180 °C) of the (SI2VP-13)/Cloisite 30B® nanocomposite (see Fig. 18), the CSC microdomains of SI2VP-13 in region I become disordered, thus greatly enhancing the mobility of the SI2VP-13 chains. Under such circumstances, the P2VP blocks of SI2VP-13 can easily diffuse to the surface of an organoclay and interact with the N^+ ions, resulting in an increase in the number of tethered chains on the organoclay platelets. Therefore, the probability of forming aligned organoclay platelets along a specific direction (or the volume of region II) is expected to increase, which in turn will make the SAXS profiles appear at q^* ratios of 1: 2: 3: 4.

Interestingly, as can be seen from Fig. 16, the values of G' for the (SI2VP-13)/Cloisite 30B® nanocomposite decrease very rapidly during heating from 120 °C and then go through a minimum at 180 °C followed by a very rapid increase as the heating continues to about 220 °C. Therefore we conclude that the rapidly increasing trend of G' near 180 °C, representing the T_{ODT} of the (SI2VP-13)/Cloisite 30B® nanocomposite observed in Fig. 16, is due to the existence of organoclay platelets being aligned along a specific direction.

Fig. 18b gives SAXS profiles at various temperatures during heating from 120 to 220 °C for (SI2VP-13)/Cloisite 30B® nanocomposite specimens which were prepared by melt blending at an extruder barrel temperature of 200 °C for 6 min. It is seen that at temperatures above 180 °C the temperature dependence of the SAXS profiles (having the Bragg spacings in the following ratios, 1: 2: 3: 4) in Fig. 18b is very similar to that observed in Fig. 18a. However, in Fig. 18b we observe an additional scattering peak near $3q^*$ (marked by the arrow) at lower temperatures (120–160 °C), although the peak height is small. Notice that this scattering peak is not discernible in Fig. 18a. This observation seems to indicate that the amount of aligned organoclay platelets along a specific direction (or the volume of region II) is larger than that in the sample prepared by melt blending at 160 °C, which is due to a higher mobility of P2VP chains to interact with N^+ ions at higher temperatures. This difference between the two might explain the reason why, referring to Fig. 16, values of G' for the specimen that was melt-blended at 200 °C are slightly larger than those for the specimen that was melt-blended at 160 °C.

3.5. Dispersion characteristics of melt-blended organoclay nanocomposite based on microphase-separated high-molecular-weight SI2VP-3H

An organoclay nanocomposite based on a high-molecular-weight SI2VP-3H was prepared by melt blending with Cloisite 15A® at an extruder barrel temperature of 180 °C for 6 min using a twin-screw mini-compounder. Note from Fig. 1 that the T_{ODT} of SI2VP-3H is much higher than 220 °C. Fig. 19 gives an XRD pattern of (SI2VP-3H)/Cloisite 15A® nanocomposite showing a reflection peak at about 5°, suggesting a low degree of dispersion of Cloisite 15A® aggregates in the nanocomposite. Fig. 20a gives a TEM image of neat SI2VP-3H showing lamellar microdomains with alternating layers of PS phase (the bright areas) and PI phase (the dark areas

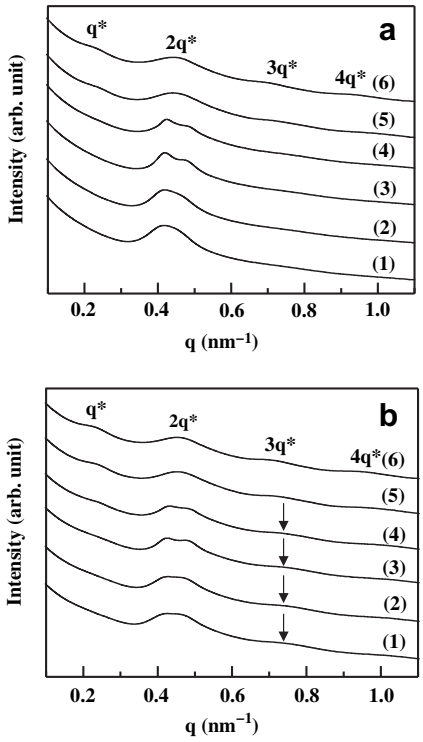

Fig. 18. SAXS profiles of (SI2VP-13)/Cloisite 30B® nanocomposites, which were melt blended for 6 min in a twin-screw mini-compounder at a screw speed of 180 rpm at two different temperatures, (a) 160 °C and (b) 200 °C, at various temperatures (°C): (1) 120, (2) 140, (3) 160, (4) 180, (5) 200, and (6) 220.

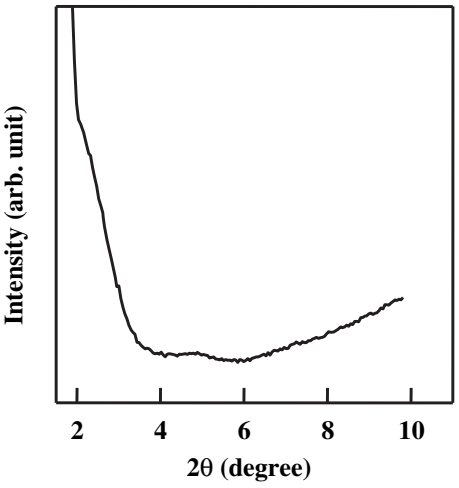

Fig. 19. XRD patterns of (SI2VP-3H)/Cloisite 15A® nanocomposite which was prepared by melt blending at an extruder barrel temperature of 180 °C for 6 min in a twin-screw mini-compounder at a screw speed of 180 rpm.

due to the staining with osmium tetroxide). The lamellar microdomain of SI2VP-3H is expected, because it can be regarded as being effectively a compositionally symmetric SI diblock copolymer owing to very small amounts (3 wt%) of P2VP block present in SI2VP-3H. Fig. 20b gives a TEM image of (SI2VP-3H)/Cloisite 15A® nanocomposite without the PI block stained, in which the dark areas represent the aggregates of Cloisite 15A® and the grey areas represent the matrix of SI2VP-3H, showing that the aggregates of Cloisite 15A® are bundled together in the matrix of SI2VP-3H. Fig. 20c gives a TEM image of (SI2VP-3H)/Cloisite 15A® nanocomposite with the PI block stained using osmium tetroxide, showing that the lamellar microdomains present in neat SI2VP-3H (see Fig. 20a) are very much disrupted in the presence of large aggregates of Cloisite 15A®. Thus we conclude that the dispersion characteristics of (SI2VP-3H)/Cloisite 15A® nanocomposite is very poor. The difference in the degree of dispersion of the organoclay aggregates between the melt-blended (SI2VP-13)/Cloisite 30B® nanocomposite (see Fig. 15) and melt-blended (SI2VP-3H)/Cloisite 15A® nanocomposite (see Fig. 20c) is ascribed to the difference in the melt blending temperature employed in relation to the T_{ODT} of the respective block copolymers, SI2VP-13 and SI2VP-3H.

Since we could not experimentally determine the T_{ODT} of SI2VP-3H, using the mean field theory of Helfand and Wasserman [37], we estimated the T_{ODT} of SI2VP-3H to be about 360 °C on the basis of the following approximation; namely since at present there exists no theory enabling us to predict the T_{ODT} of an ABC-type triblock copolymer and the amount of P2VP block in SI2VP-3H is only 3 wt%, we approximated the triblock copolymer SI2VP-3H as a PS-*block*-PI (SI diblock) copolymer. Then, in estimating the T_{ODT} of the SI diblock copolymer equivalent to SI2VP-3H, we used the following expression for the temperature-dependent interaction parameter [41]:

$$\alpha = -1.18 \times 10^{-3} + 0.839/T \quad (1)$$

for PS/PI pair, where α is related to the Flory–Huggins interaction parameter χ by $\chi = \alpha V_{ref}$ with V_{ref} being the molar volume of a reference component. Now it should be clear why we could not prepare, via melt blending, (SI2VP-3H)/Cloisite 15A® nanocomposite at temperatures above the estimated T_{ODT} (360 °C) of SI2VP-3H without inducing severe thermal degradation/cross-linking of the PI block in SI2VP-3H.

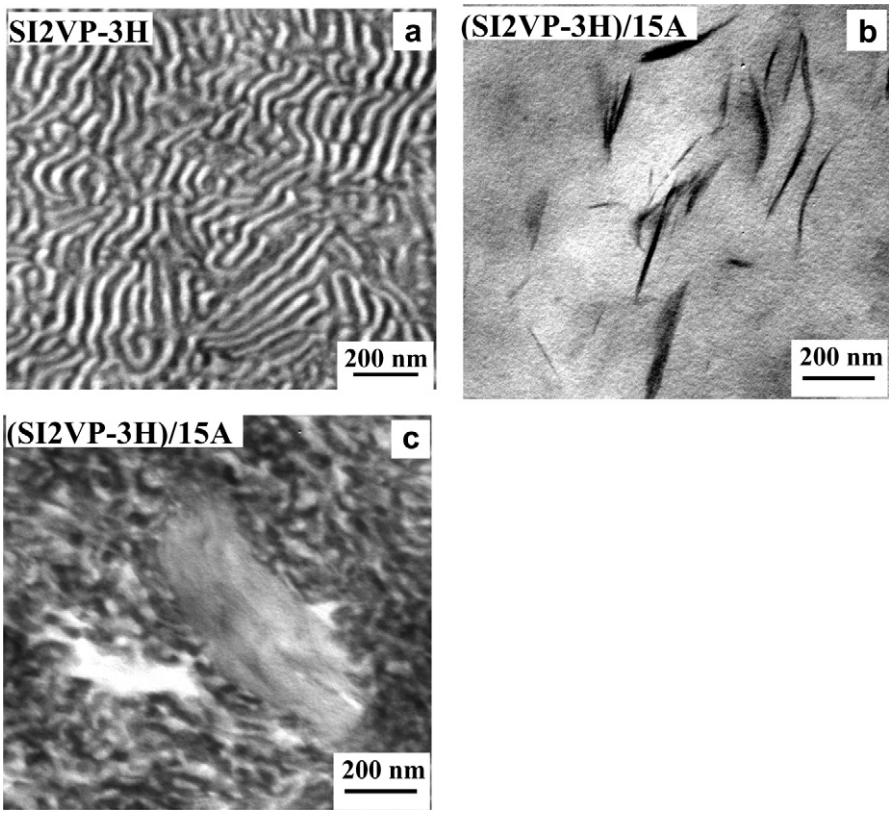

Fig. 20. TEM images of (a) neat SI2VP-3H with the PI phase stained with osmium tetroxide, (b) melt-blended (SI2VP-3H)/Cloisite 15A® nanocomposite without staining, and (c) melt-blended (SI2VP-3H)/Cloisite 15A® nanocomposite with the PI phase stained with osmium tetroxide. The nanocomposite samples were prepared by melt blending at an extruder barrel temperature of 180 °C for 6 min in a twin-screw mini-compounder at a screw speed of 180 rpm.

Note that the weight-average molecular weight (M_w) of SI2VP-3H is 9.63×10^4 (see Table 1), which is about three times higher than the molecular weight ($M_w = 2.47 \times 10^4$) of SI2VP-13. If we consider, for simplicity, that both block copolymers are in the disordered state (at $T > T_{ODT}$) and they are entangled polymers, we can estimate that the melt viscosity of SI2VP-3H would be about 100 times higher than that of SI2VP-13, using the relationship $\eta \propto M^{3.4}$ which is only valid for flexible, entangled homopolymers. However, the melt viscosity of a block copolymer in the microphase-separated state (at $T < T_{ODT}$) would be very high as compared to that in the disordered state (at $T > T_{ODT}$). Needless to say, values of melt viscosity of a microphase-separated block copolymer depend on how far the measurement temperature lies below its T_{ODT}. For instance, when the measurement temperature is very far (say 100 °C) below the T_{ODT} of a microphase-separated block copolymer, its melt viscosity would be extremely high as compared to that at temperatures slightly (say 10 °C) below its T_{ODT}.

One may ask: What does the melt viscosity of a block copolymer have anything to do with determining the degree of dispersion of the aggregates of organoclay in the preparation of nanocomposites by melt blending? The answer to the question lies in that the more viscous a block copolymer, the less chance there will be for the block copolymer to have intimate contacts with an organoclay during melt blending. Thus we conclude that the melt viscosity of a block copolymer through its molecular weight and thus through T_{ODT} would play a very significant role in determining the degree of dispersion of the aggregates of organoclay during the preparation of nanocomposites by melt blending. It is then not difficult to understand the reason why the (SI2VP-3H)/Cloisite 15A® nanocomposite prepared by melt blending at an extruder barrel temperature of 180 °C, which is about 180 °C below the estimated T_{ODT} of SI2VP-3H, has very poor dispersion of the aggregates of Cloisite 15A® (see Fig. 20b and c).

We are aware of some literature [42–45] which reported on the effect of molecular weight on the mechanical properties of organoclay nanocomposites based on commercial homopolymer (e.g., high-density polyethylene; polypropylene; and nylon 6). Some research groups [42–44] reported that the mechanical properties of the nanocomposites prepared increased with increasing molecular weight of polymer matrix while very poorly intercalated morphology was observed. We are of the opinion that there is no physical significance to discuss the mechanical properties of poorly intercalated nanocomposites. When exfoliated organoclay nanocomposites were observed with increasing molecular weight of nylon 6 matrix [45], the authors did not offer a plausible physicochemical mechanism supported by independent experiment. We are of the opinion that the increased melt viscosity (or shear stress) alone arising from higher molecular weight could not adequately explain the reason of the exfoliation of the clay platelets.

3.6. Dispersion characteristics of melt-blended organoclay nanocomposites based on a functionalized commercial block copolymer

There are very few commercial block copolymers that have functionality. In the present study we prepared, via melt blending, an organoclay nanocomposite based on a functional block copolymer (FG-1901X, Kraton Products Company), which is a commercial polystyrene-*block*-poly(ethylene-*co*-2-butene)-*block*-polystyrene (SEBS triblock) copolymer grafted with 1.7 wt% maleic anhydride (MA) onto the poly(ethylene-*co*-1,2-butene) (PEB) block. This block copolymer, which will be referred to as SEBS-*g*-MA, has $M_w = 5.6 \times 10^4$ and a polydispersity index of 1.06 as determined by GPC against polystyrene standards. In the preparation of a nanocomposite based on SEBS-*g*-MA, Cloisite 15A® was employed, and a twin-screw mini-compounder was utilized at an extruder barrel temperature of 220 °C and at a screw speed of 180 rpm for 8 min.

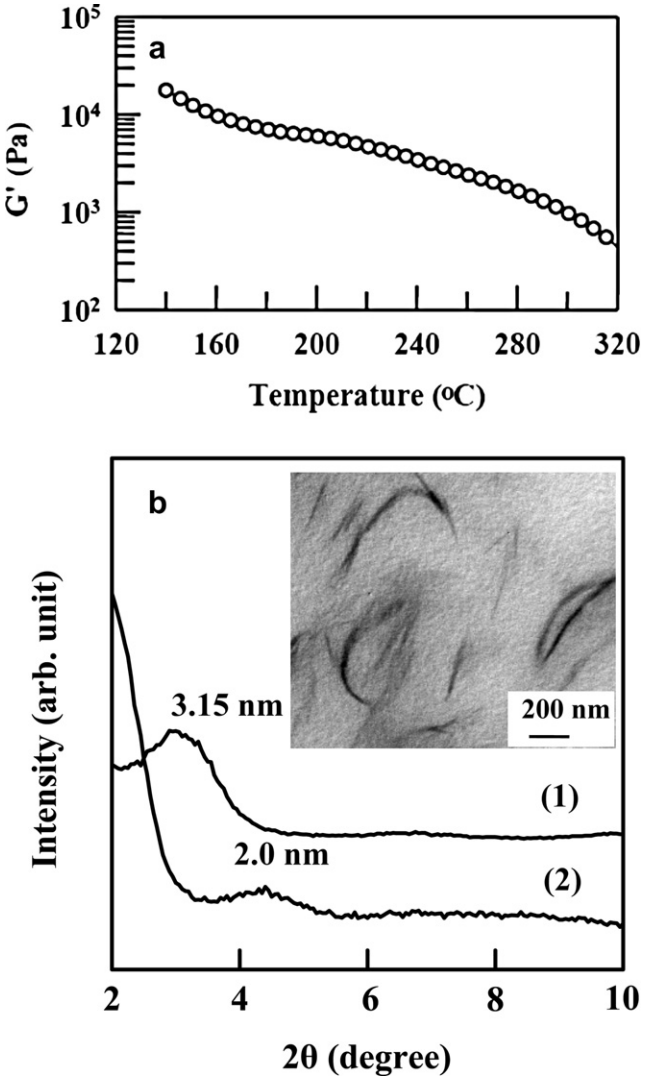

Fig. 21. (a) Variations of G' with temperature for SEBS-*g*-MA during the isochronal dynamic temperature sweep experiments at an angular frequency of 0.01 rad/s. (b) XRD patterns of (1) Cloisite 15A® and (2) melt-blended (SEBS-*g*-MA)/Cloisite 15A® nanocomposite in which the inset shows a TEM image of (SEBS-*g*-MA)/Cloisite 15A® nanocomposite. The nanocomposite specimen was prepared by melt blending at an extruder barrel temperature of 220 °C for 8 min in a twin-screw mini-compounder at a screw speed of 180 rpm.

Fig. 21 gives (a) variations of G' with temperature for SEBS-*g*-MA during isochronal dynamic temperature sweep experiments at $\omega = 0.1$ rad/s and (b) XRD patterns for (1) neat Cloisite 15A® and (2) (SEBS-*g*-MA)/Cloisite 15A® nanocomposite. The following observations are worth noting in Fig. 21. Fig. 21a shows that SEBS-*g*-MA has a T_{ODT} much higher than 320 °C, the highest experimental temperature employed, and Fig. 21b shows that the XRD pattern of (SEBS-*g*-MA)/Cloisite 15A® nanocomposite has a conspicuous reflection peak at a d-spacing of 2.0 nm, while the XRD pattern of neat Cloisite 15A® has a d-spacing of 3.15 nm. It is interesting to observe from the XRD patterns given in Fig. 21b that the *d*-spacing of Cloisite 15A® in the nanocomposite is smaller than that of neat Cloisite 15A®. This observation may be due to the detachment, during melt blending, of some of the surfactant residing at the surface of Cloisite 15A® in the nanocomposite. The XRD pattern of (SEBS-*g*-MA)/Cloisite 15A® nanocomposite suggests that it might

have poor dispersion of the aggregates of Cloisite 15A®. Indeed, the TEM image given in the inset of Fig. 21b shows poor dispersion of the aggregates of Cloisite 15A® in the (SEBS-*g*-MA)/Cloisite 15A® nanocomposite.

The poor dispersion of the aggregates of Cloisite 15A® in the matrix of SEBS-*g*-MA observed in Fig. 21b should not be surprising for the following reasons. According to the previous study of Choi et al. [24], the presence of a functional group in the midblock of an ABA-type triblock copolymer would not be effective, while the presence of a functional group in the endblock would be very effective, in dispersing the aggregates of an organoclay in the matrix of an ABA-type triblock copolymer. Further, the melt blending temperature chosen, 220 °C, which was very far below the T_{ODT} (>320 °C) of SEBS-*g*-MA, contributed to the very poor dispersion of the aggregates of Cloisite 15A® in the (SEBS-*g*-MA)/Cloisite 15A® nanocomposite, because the melt viscosity of the microphase-separated SEBS-*g*-MA at 220 °C must have been extremely high, severely restricting the mobility of SEBS-*g*-MA chains toward the surface of organoclay Cloisite 15A® in the nanocomposite.

4. Concluding remarks

In the present study, using TEM we have identified the location of exfoliated organoclay platelets in the nanocomposite based on microphase-separated SI2VP triblock copolymer; namely, they reside in the PI phase of a microphase-separated SI2VP triblock copolymer (SI2VP-13). We have found that due to the presence of exfoliated organoclay platelets in the PI phase, the CSC microdomains of neat SI2VP-13 has transformed to lamellar microdomains inside two neighboring organoclay platelets. The observed phase transformation is attributable to a change in curvature of the interfaces between the constituent components, which was driven by the strong attractive interactions, via ion–dipole interactions, between the positively charged N^+ ion in a surfactant residing at the surface of an organoclay and the polar pyridine ring in the P2VP block of the SI2VP triblock copolymer [26].

In the present study, we have demonstrated a very important concept from the processing point of view that melt blending temperature must be chosen to be higher than the T_{ODT} of a block copolymer in order to prepare exfoliated nanocomposites based on microphase-separated block copolymers. This is because when the melt blending temperature is very far below the T_{ODT} of a microphase-separated block copolymer, its melt viscosities would be extremely high, hindering intimate mixing (or contacts) between the block copolymer and organoclay and thus giving rise to poor dispersion of the aggregates of organoclay. This problem does not exist when solution blending is used to prepare nanocomposites. This concept is very similar to the situation where effective compatibilization of two immiscible homopolymers or random copolymers using a block copolymer can only be realized if the melt blending temperature is chosen to be higher than the T_{ODT} of the block copolymer [46].

The requirement that the melt blending temperature must be higher than the T_{ODT} of a block copolymer to prepare exfoliated organoclay nanocomposites is still valid even when strong attractive interactions exist between the block copolymer and organoclay chosen. Since most of the commercial block copolymers have very high T_{ODT} owing to very high molecular weight, exfoliation of melt-blended organoclay nanocomposites based on such commercial block copolymers is unlikely to occur for the reasons presented in this paper. It is then no surprise that a study has not yet been reported on the preparation of exfoliated organoclay nanocomposites based on commercial block copolymers, which were prepared by melt blending. The above observations have profound implications, conceptually and practically, in that the presence of strong attractive interactions between a block copolymer and organoclay alone is not sufficient, although necessary, for a block copolymer to exfoliate the aggregates of an organoclay during melt blending.

In this study, we have found that the molecular weight of a block copolymer (SI2VP-13 versus SI2VP-3H) also plays an important role in determining whether exfoliation or intercalation of the aggregates of an organoclay would occur. This problem is far less serious when solution blending is used to prepare organoclay nanocomposites.

Acknowledgment

C. D. Han acknowledges with gratitude that this study was supported in part by the National Science Foundation under Grant CST-0406752. J. K. Kim acknowledges the support of the National Creative Research Initiative Program by the National Research Foundation (NRF) of Korea and the second stage of the BK21 program of Korea. Synchrotron small-angle X-ray scattering experiments were performed at PLS beamlines 4C1 and 10C1 supported by POSCO and NRF.

References

[1] Ray SS, Okamoto M. Prog Polym Sci 2003;28:1539.
[2] Moet A, Akelah A. Mater Lett 1993;18:97.
[3] Akelah A, Moet A. J Mater Sci 1996;31:3589.
[4] Hasegawa N, Okamoto H, Kawasumi M, Usuki A. J Appl Polym Sci 1999;74:3359.
[5] Hoffmann B, Dietrich C, Thomann R, Friedrich C, Mülhaupt R. Macromol Rapid Commun 2000;21:57.
[6] Beyer FL, Beck Tan NC, Dasgupta A, Galvin ME. Chem Mater 2002;14:2988.
[7] Kato M, Usuki A, Okada A. J Appl Polym Sci 1997;66:1781.
[8] Kawasumi M, Hasegawa N, Kato M, Usuki A, Okada A. Macromolecules 1997;30:6333.
[9] Liu X, Wu Q. Polymer 2001;42:10013.
[10] Nam PH, Maiti P, Okamoto M, Kotaka T, Hasegawa N, Usuki A. Polymer 2001;42:9633.
[11] Lee KM, Han CD. Polymer 2003;44:4573.
[12] Yoon PJ, Hunter DL, Paul DR. Polymer 2003;44:5323.
[13] Yoon PJ, Hunter DL, Paul DR. Polymer 2003;44:534.
[14] Liu YJ, Schindler JL, DeGroot DC, Kannewurf CR, Hirpo W, Kanatzidis MG. Chem Mater 1996;8:525.
[15] Aranda P, Ruiz-Hitzky E. Chem Mater 1992;4:1396.
[16] Bujdák J, Hackett E, Giannelis EP. Chem Mater 2000;12:2168.
[17] Jimenez G, Okata N, Kawai H, Ogihara T. J Appl Polym Sci 1997;64:2211.
[18] Di Y, Iannace S, Di Maio E, Nicolais L. J Polym Sci Polym Phys Ed 2003;41:670.
[19] Grim RE. Clay minerology. 2nd ed. New York: McGraw Hill; 1968.
[20] Theng BK. The chemistry of clay-organic reactions. New York: Wiley; 1974.
[21] Zhao H, Shipp DA. Chem Mater 2003;15:2693.
[22] Di J, Sogah DY. Macromolecules 2006;39:5052.
[23] Lee KM, Han CD. Macromolecules 2003;36:804.
[24] Choi S, Lee KM, Han CD. Macromolecules 2004;37:7649.
[25] Zha W, Choi S, Lee KM, Han CD. Macromolecules 2005;38:8418.
[26] Zha W, Han CD, Han SH, Lee DH, Kim JK, Guo M, et al. Polymer 2009;50:2411.
[27] Ha YH, Kwon Y, Breiner T, Chan EP, Tzianetopoulou T, Cohen RE, et al. Macromolecules 2005;38:5170.
[28] Mitchell CA, Krishnamoorti R. J Polym Sci Polym Phys Ed 2002;40:1434.
[29] Ha YH, Thomas EL. Macromolecules 2002;35:4419.
[30] Liao M, Zhu J, Xu H, Li Y, Shan W. J Appl Polym Sci 2004;92:3430.
[31] Silva AS, Mitchell CA, Tse MF, Wang HC, Krishnamoorti R. J Chem Phys 2001;115:7166.
[32] Chen H, Schmidt DF, Pitsikalis M, Hadjichristidis N, Zhang Y, Wiesner U, et al. Polym Sci Polym Phys Ed 2003;41:3264.
[33] Hasegawa N, Usuki A. Polym Bull 2003;51:77.
[34] Physical Properties Bulletin from Southern Clay Products.
[35] Gouinlock EV, Porter RS. Polym Eng Sci 1977;17:535.
[36] Leibler L. Macromolecules 1980;13:1602.
[37] Helfand E, Wasserman ZR. Developments in block copolymers. In Goodman I, editor. Applied science, New York; 1982, [chapter 4].
[38] Bailey TS, Pham HD, Bates FS. Macromolecules 2001;34:6994.
[39] Hashimoto T, Shibayama M, Kawai K. Macromolecules 1980;13:1237.
[40] Choi SB, Vaidya NY, Han CD, Sota N, Hashimoto T. Macromolecules 2003;36:7707.
[41] Han CD, Baek DM, Kim JK. Macromolecules 1990;23:561.
[42] Chu D, Nguyen Q, Baird DG. Polym Compos 2007;28:499.
[43] Wang Y, Chen FB, Wu KC. J Appl Polym Sci 2005;97:1667.
[44] Wang Y, Chen FB, Wu KC, Wang JC. Polym Eng Sci 2006;46:289.
[45] Fornes TD, Yoon PJ, Keskkula H, Paul DR. Polymer 2001;42:9929.
[46] Chun SB, Han CD. Macromolecules 1999;32:4030.